

Electronic Supplementary Information for:

***t₁-Noise Eliminated Dipolar Heteronuclear Multiple-Quantum Coherence
Solid-State NMR Spectroscopy***

Amrit Venkatesh,^{1,2} Xuechen Luan,¹ Ivan Hung,³ Frédéric A. Perras,² Wenyu Huang,^{1,2} Aaron J. Rossini^{1,2*}

¹ *Iowa State University, Department of Chemistry, Ames, IA, USA, 50011*

² *US DOE Ames Laboratory, Ames, Iowa, USA, 50011*

³ *National High Magnetic Field Laboratory (NHMFL), Tallahassee, FL, USA, 32310*

Table of Contents

Supplementary Information	Page
Details on Monte Carlo simulations of t_1 -noise	3
Note S1: Estimation of f_{corr} for histidine	5
Figure S1: Plot showing experimental variation of MAS frequency	6
Figure S2: 2D $^1\text{H}\{^{35}\text{Cl}\}$ D-HMQC spectra of histidine acquired without population transfer at 9.4 T	7
Figure S3: SIMPSON simulations with ^1H recoupled echo pulse sequences	8
Figure S4: SIMPSON simulations of TONE D-HMQC-1 (effect of X π pulses)	9
Figure S5: Variation of $^1\text{H}\{^{35}\text{Cl}\}$ (TONE) D-HMQC signal intensity with LG spinlock/echo duration	10
Figure S6: Comparison of 1D TONE D-HMQC-3 and 4 spectra with two rotor cycle LG spin-lock pulses	11
Figure S7: TONE D-HMQC-5 pulse sequence and spectrum	12
Figure S8: $^1\text{H}\{^{35}\text{Cl}\}$ D-HMQC spectra at 18.8 T	13
Figure S9: Incorporation of population transfer scheme in TONE D-HMQC	14
Figure S10: 2D $^1\text{H}\{^{35}\text{Cl}\}$ D-HMQC spectra with population transfer at 9.4 T	15
Figure S11: $^1\text{H}\{^{35}\text{Cl}\}$ TONE D-HSQC spectra	16
Figure S12: Comparison of signal decay with TONE D-HSQC and conventional D-HMQC	17
Figure S13: PXRD and ^1H spin echo spectrum of LDH	18
Figure S14: $^1\text{H}\{^{25}\text{Mg}\}$ PT TONE D-HMQC-3 with short recoupling time of LDH	19
Figure S15: 1D $^1\text{H}\{^{27}\text{Al}\}$ spectra ^{27}Al traces from 2D spectra acquired D-HMQC, D-HSQC and D-RINEPT pulse sequences of LDH	20
Figure S16: 2D $^1\text{H}\{^{27}\text{Al}\}$ spectra acquired with D-HMQC, D-HSQC and D-RINEPT pulse sequences of LDH	21
Figure S17: Comparison 2D $^1\text{H}\{^{25}\text{Mg}\}$ conventional and TONE D-HMQC spectra of LDH	22
Figure S18: $^1\text{H}\{^{25}\text{Mg}\}$ TONE D-HMQC-4 spectrum of LDH	23
Figure S19: 2D $^1\text{H}\{^{25}\text{Mg}\}$ D-HMQC spectra of Magnesium Hydroxide	24
Figure S20: Comparison of 2D $^1\text{H}\{^{13}\text{C}\}$ conventional and TONE D-HMQC spectra of histidine	25
Supplementary Tables	
Tables S1-S22: Lorentz/Gauss fits of SIMPSON MAS profiles	26-38

Monte Carlo simulations of t_1 -noise.

The MATLAB code used to simulate the variation of t_1 -noise in 2D HMQC experiments performs the following steps: (i) A Gaussian probability function is used to randomize the MAS frequency for each scan. The central MAS frequency (here 50000 Hz) and the standard deviation (σ_{MAS}) are input. The probability (p) of a given MAS frequency (ν_{MAS}) is given by:

$$p(\nu_{MAS}) = \exp\left(-\frac{1}{2}\left(\frac{\nu_{MAS} - 50000\text{Hz}}{\sigma_{MAS}}\right)^2\right)$$

A small value of σ_{MAS} corresponds to stable spinning, while a large value corresponds to unstable spinning. (ii) The randomly generated MAS frequency from step (i) and the intensity-MAS frequency profiles for a given δ_{aniso} obtained from SIMPSON simulations are used to calculate the scaling factors for the correlated and uncorrelated signals (s_{corr} and s_{uncorr} , respectively) for the n^{th} scan:

$$s_{corr}^n(\nu_{MAS}) = \exp\left(-\frac{1}{2}\left(\frac{\nu_{MAS} - 50000\text{Hz}}{\Gamma_{g,corr}}\right)^2\right) \times \left(\frac{\left(\frac{1}{2}\Gamma_{l,corr}\right)^2}{(\nu_{MAS} - 50000)^2 + \left(\frac{1}{2}\Gamma_{l,corr}\right)^2} \right)$$

$$s_{uncorr}^n(\nu_{MAS}) = \left(\exp\left(-\frac{1}{2}\left(\frac{\nu_{MAS} - 50000\text{Hz}}{\Gamma_{g,uncorr}}\right)^2\right) \times \left(\frac{\left(\frac{1}{2}\Gamma_{l,uncorr}\right)^2}{(\nu_{MAS} - 50000)^2 + \left(\frac{1}{2}\Gamma_{l,uncorr}\right)^2} \right) \right) - (1 - I_0)$$

The correlated and uncorrelated signal intensity profiles from SIMPSON were fit to mixed Gaussian and Lorentzian functions to simplify the calculation of s_{corr} and s_{uncorr} . Γ_g and Γ_l are the fitted widths of the Gaussian and Lorentzian components, respectively (Table S1-S22). In addition, an offset term ($1 - I_0$) is added to s_{uncorr} to match the amplitude offset of the uncorrelated signal intensity (Figure 2C and 2D). (iii) The scaling factors from step (ii) are applied to the respective correlated and uncorrelated time domain signal functions to calculate the correlated and uncorrelated time domain signal intensities for each scan:

$$S_{corr}^n(\nu_{MAS}, t_1) = f_{corr} \times s_{corr} \times \left(\exp\left(-\left(\frac{t_1}{T_{2,corr}}\right)^2\right) \right)$$

$$S_{uncorr}^n(\nu_{MAS}, t_1) = (1 - f_{corr}) \times s_{uncorr} \times \left(\exp\left(-\left(\frac{t_1}{T_{2,uncorr}}\right)^2\right) \right) \times (-1)^n$$

The correlated time domain signal intensity function (S_{corr}^n) is calculated from a simple Gaussian function of t_1 , with a decay constant ($T_{2,corr} = 1/R_{2,corr}$) given by sum of the refocused ${}^1\text{H}$ transverse relaxation rate (R_2') and X inhomogeneous relaxation rate ($R_2^* = 1/T_2^*$). Here, $R_2^* = 4$ kHz, $R_2' = 2$ kHz and $R_{2,corr} = 6$ kHz. The Gaussian function was chosen to minimize truncation artefacts upon Fourier transformation. The uncorrelated time domain signal (S_{uncorr}^n) is calculated from a Lorentzian function that decays under ${}^1\text{H}$ T_2' only. Note that the sign of S_{uncorr}^n alternates on each scan (given by -1 exponentiated by the scan index, n) to mimic the (partial) cancellation of

uncorrelated signals by phase cycling. f_{corr} is an adjustable parameter that gives the amplitude of the HMQC signal as compared to the uncorrelated or background signal. For the simulations in Figures 2E-2H, f_{corr} was set to 0.05 and was held constant for all scans and t_1 -points. For comparison, f_{corr} was estimated to be between 0.05 and 0.11 for the $^1\text{H}\{^{35}\text{Cl}\}$ D-HMQC experiments on histidine (see Note S1). (iv) The final time domain intensity for each t_1 -point was then calculated by adding together S_{corr}^n and S_{uncorr}^n for all scans (here 16):

$$S(t_1) = \sum_{n=1}^{n=16} \left\{ S_{corr}^n(v_{MAS}, t_1) + S_{uncorr}^n(v_{MAS}, t_1) \right\}$$

(v) The indirect dimension evolution time (t_1) was then incremented (here, $\Delta t_1 = 10 \mu\text{s}$) and the procedure outlined above was repeated for the total number of t_1 -points (here 500) to calculate an FID with t_1 -noise. (vi) Random (thermal) noise was then added to obtain a final noised FID. The addition of thermal noise makes the quantification of the signal-to-noise ratio (SNR) more reliable. Thermal noise was added so that the SNR was 95 in the absence of t_1 -noise. For all noised FIDs, SNR was measured in the frequency domain after Fourier transformation.

NOTE S1. The estimation of f_{corr} which was used to scale the correlated time domain signal intensity is described here.

- (i) Since ^{35}Cl is a spin-3/2 quadrupolar nucleus, only 50% of spins, which reside in the central transition (CT), are observable with CT selective pulses. This step results in $f_{corr} = 0.5$.
- (ii) 75% natural abundance results in reduction of observable ^{35}Cl spins to 0.75×0.5 , which results in $f_{corr} = 0.375$.
- (iii) For conventional D-HMQC, we have measured the experimental dipolar recoupling efficiency to be *ca.* 15-30%. The dipolar recoupling efficiency was measured with respect to a 1D ^1H spin echo spectrum. This results in f_{corr} of 0.056 (0.15×0.375) to 0.11 (0.3×0.375) depending on the efficiency. The experimental efficiency with population transfer improves roughly by a factor 2 which should aid in reducing the uncorrelated signal fraction to some extent.

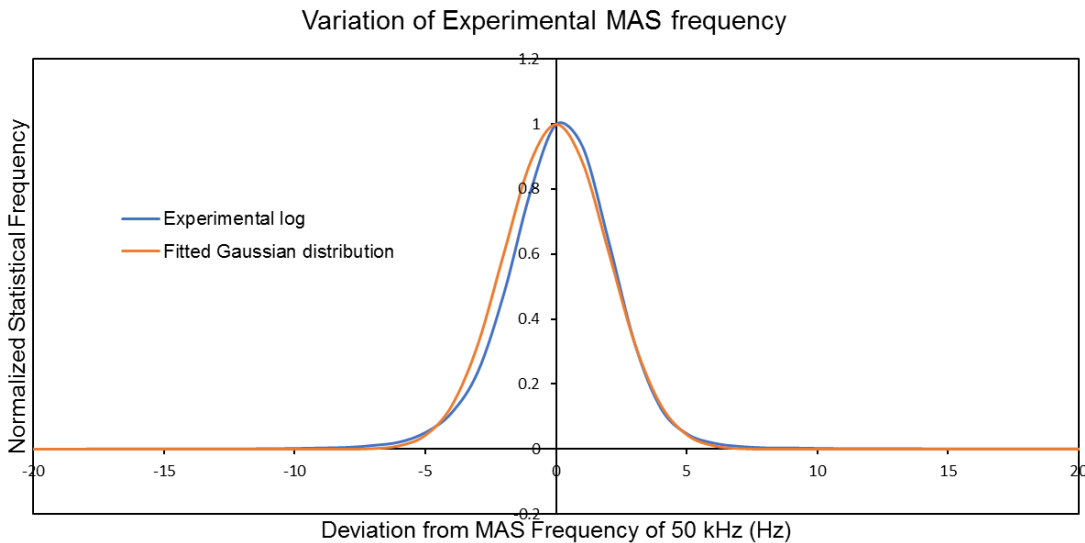


Figure S1. Plot showing the variation of the normalized statistical frequency with the deviation from set MAS frequency of 50 kHz over a 20 hour period. The MAS frequency readout from the Bruker MAS-3 interface on Topspin 3.5 pl3 was recorded every second. The normalized statistical frequency is defined as the number of times an arbitrary MAS frequency value is repeated in the data set. Fitting the experimental distribution to a Gaussian function yields an estimate for $\sigma_{\text{MAS}} = 2 \text{ Hz}$. Note that the recorded MAS frequency is likely an average over an undefined amount of time ($< 1\text{s}$) and the real variation of MAS frequency on the time-scale of a rotor period may be potentially higher.

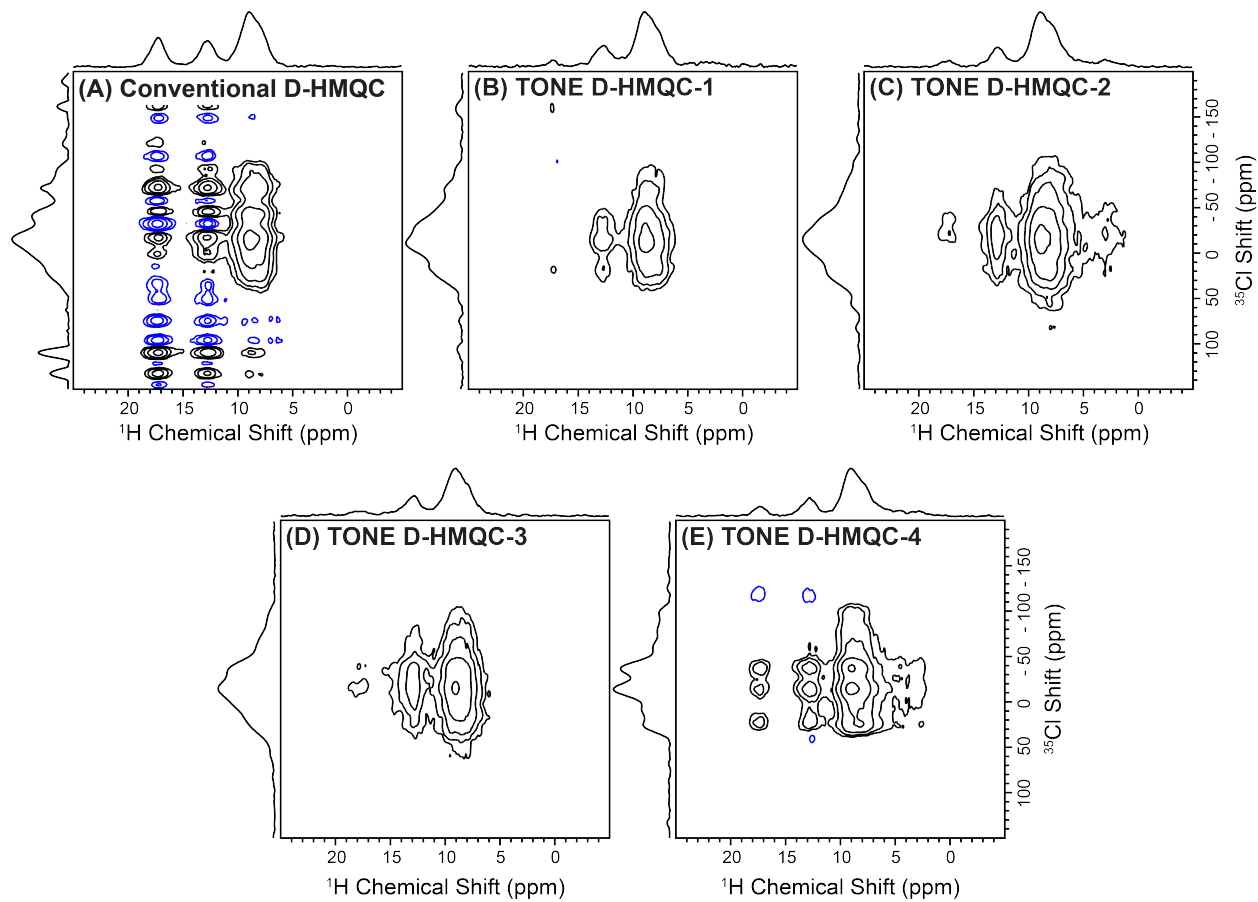


Figure S2. 2D $^1\text{H}\{\text{Cl}^{35}\}$ spectra acquired with (A) conventional D-HMQC, (B) TONE D-HMQC-1, (C) TONE D-HMQC-2, (D) TONE D-HMQC-3 and (E) TONE D-HMQC-4 pulse sequences. The 2D spectra were processed with the same contour floor level to aid the visual comparison of signal and noise. Skyline projections are shown in the ^1H and ^{35}Cl dimensions. Spectra were acquired with 50 kHz MAS and 9.4 T applied magnetic field.

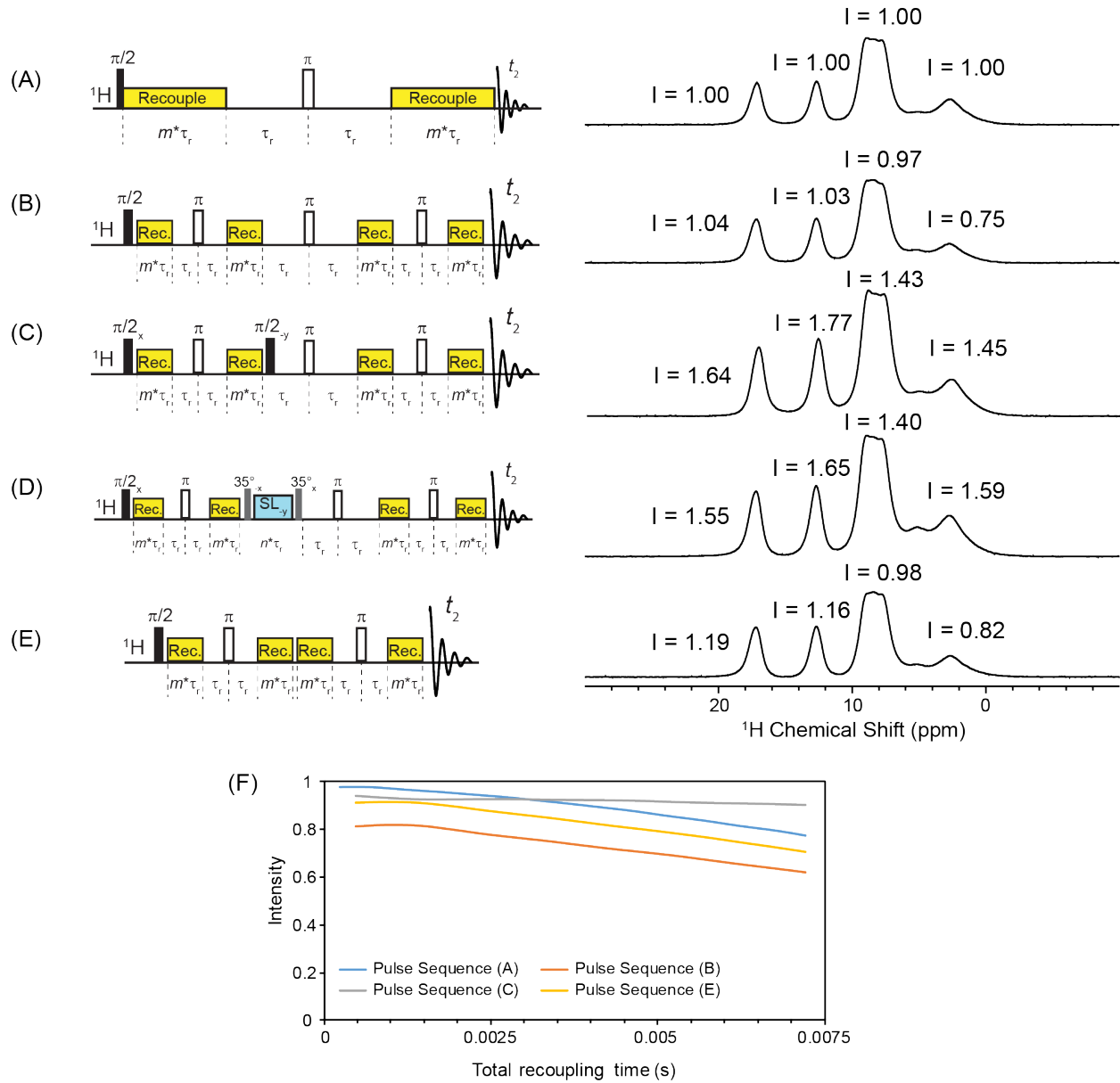


Figure S3. (A-E) (left) ¹H SR4² recoupled echo pulse sequences and (right) experimental 1D ¹H spectra obtained with a total recoupling duration of 1.92 ms (similar to the ¹H-³⁵Cl D-HMQC experiments). Recoupled echo pulse sequences shown in (A), (B), (C) and (D) are analogous to conventional D-HMQC, TONE D-HMQC-1, TONE D-HMQC-2 and TONE D-HMQC-3 pulse sequences, respectively, that are shown in the main text. The sequence shown in (E) was designed to test the impact of the central π pulse. The relative intensities of the ¹H signals are provided to aid comparison. Spectra were acquired with 50 kHz MAS and 9.4 T applied magnetic field. (F) Plot showing simulated (SIMPSON) variation of intensities with recoupling duration using the different recoupled echo sequences. Simulations were performed with two ¹H spins where the ¹H-¹H dipolar coupling was set to 15 kHz. The dephasing of ¹H signal intensities indicates that SR4² partially reintroduces ¹H-¹H couplings. However, the introduction of a π/2 pulse or a LG spin-lock pulse improves the overall efficiency of the TONE D-HMQC pulse sequences and improves robustness with respect to ¹H-¹H homonuclear dipolar couplings. The rep168 crystal file (α , β) and 16 gamma angles were used for powder averaging.

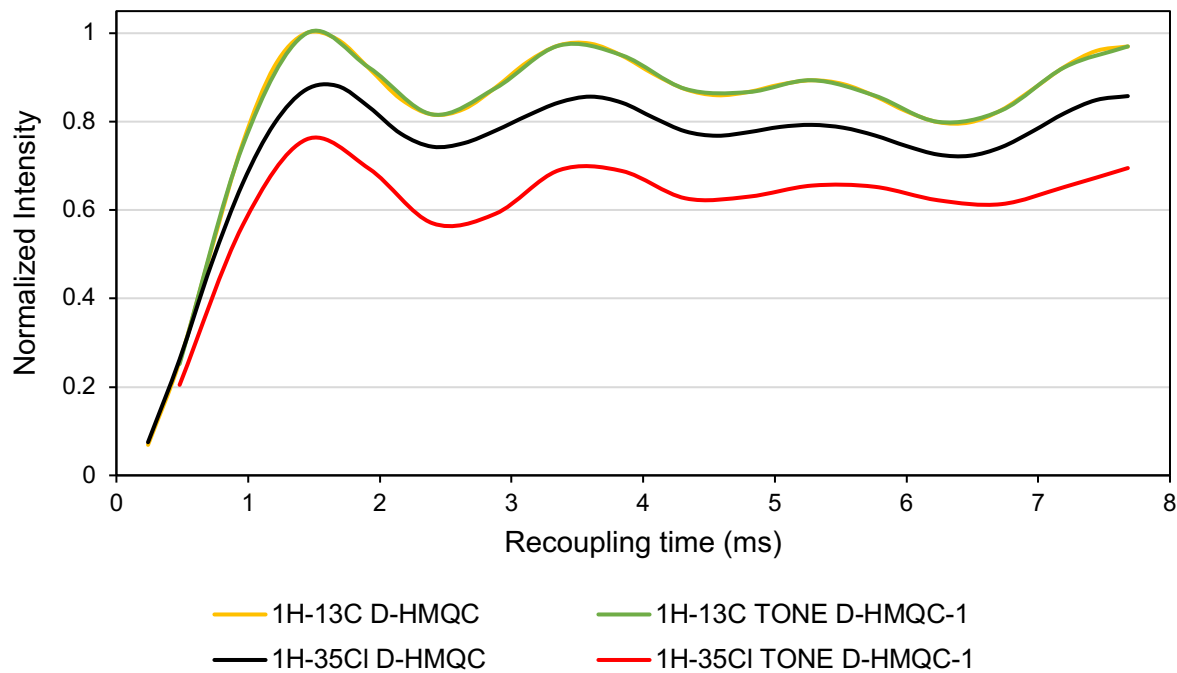


Figure S4. Plot showing the variation of SIMPSON simulated D-HMQC and TONE D-HMQC-1 intensities with recoupling duration. The curves shown in the plot correspond to (yellow) ^1H - ^{13}C D-HMQC, (green) ^1H - ^{13}C TONE D-HMQC-1, (black) ^1H - ^{35}Cl D-HMQC and (red) ^1H - ^{35}Cl TONE D-HMQC-1. The ^1H - ^{13}C simulations used 2.5 and 5 μs 90° and 180° pulses, respectively. In the ^1H - ^{35}Cl simulations, ^{35}Cl quadrupole parameters similar to histidine ($C_Q = 1.95 \text{ MHz}$ and $\eta = 0.66$) were input and 4.75 and 9.5 μs CT-selective pulses were applied on the ^{35}Cl channel. All two-spin simulations were performed with a 2 kHz heteronuclear dipolar coupling, 32 gamma angles and rep320 crystal file. The HMQC pathway was selected by filtering coherences of the order 2, 0 and -2 in all cases. All simulated curves were normalized with respect to the most intense point in the ^1H - ^{13}C D-HMQC simulation.

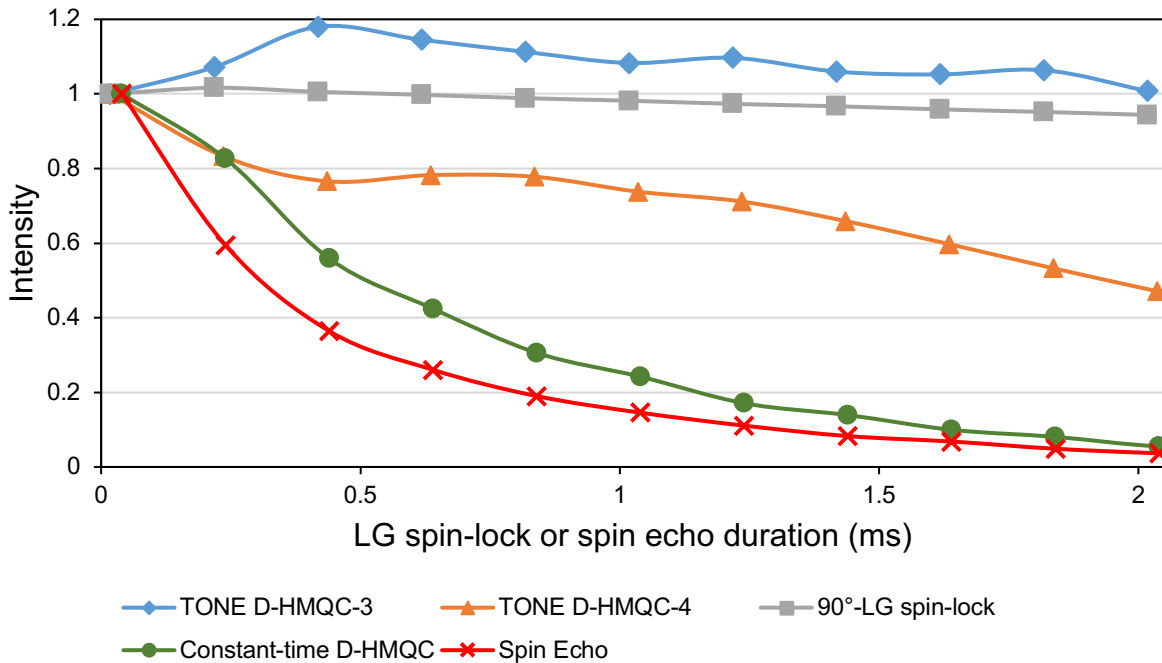
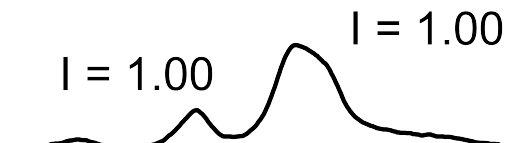
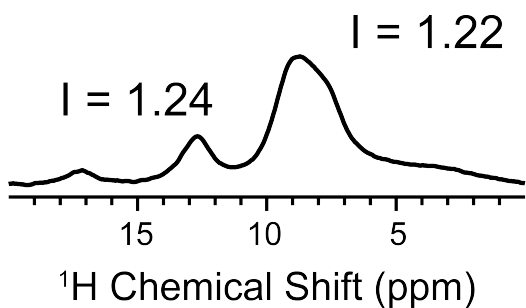


Figure S5. Plot showing variation of experimental 1D ^1H intensity with the total LG spin-lock duration using $^{1\text{H}}\{\text{Cl}^{35}\}$ TONE D-HMQC-3 (blue diamonds), $^{1\text{H}}\{\text{Cl}^{35}\}$ TONE D-HMQC-4 (orange triangles) and 90° -LG-spin-lock (grey squares). The variation of ^1H intensities with the ^1H spin echo duration in $^{1\text{H}}\{\text{Cl}^{35}\}$ constant-time D-HMQC (green circles) and ^1H spin echo (red x's) pulse sequences are also shown. The intensities are normalized with respect to the first point in each dataset. With the 90° -LG-spin-lock pulse sequence, the decay is slow as demonstrated in our previous work.¹ However, the slow residual spin diffusion during the LG spin-lock pulse may lead to signal loss as observed with TONE D-HMQC-4. This occurs when correlated spins undergo spin exchange (diffusion) with uncorrelated spins leading to imperfect refocusing by the central π pulse in TONE D-HMQC. An applied rf field of 150 kHz was used for the LG spin-lock in all cases. The signal decay in the constant-time D-HMQC and spin echo sequences is much more rapid than the decay observed with TONE D-HMQC-4 due to the shorter $^1\text{H} T_2'$ during the long echo durations. Experiments were performed at 50 kHz MAS and 9.4 T.

TONE D-HMQC-3



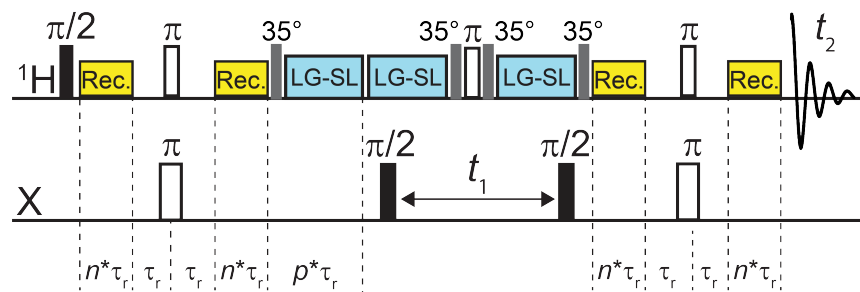
TONE D-HMQC-4



^1H Chemical Shift (ppm)

Figure S6. Comparison of 1D $^1\text{H}\{\text{Cl}^{35}\}$ TONE D-HMQC-3 and $^1\text{H}\{\text{Cl}^{35}\}$ TONE D-HMQC-4 spectra acquired with a two rotor cycle LG spin-lock pulse duration.

(A) TONE D-HMQC-5 pulse sequence



(B) TONE D-HMQC-4

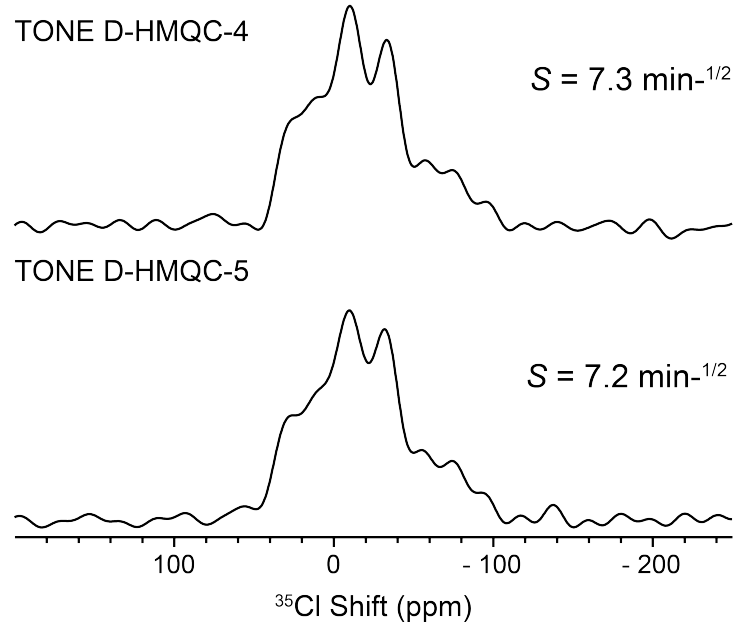


Figure S7. (A) TONE D-HMQC-5 pulse sequence featuring an incremented t_1 -period (not constant time). (B) Comparison of indirectly detected ^{35}Cl solid-state NMR spectra obtained with TONE D-HMQC-4 and TONE D-HMQC-5. Slices were extracted from 2D TONE D-HMQC-4 and -5 spectra that were acquired with a 1 s recycle delay, 16 scans and 64 TD (F_1) points.

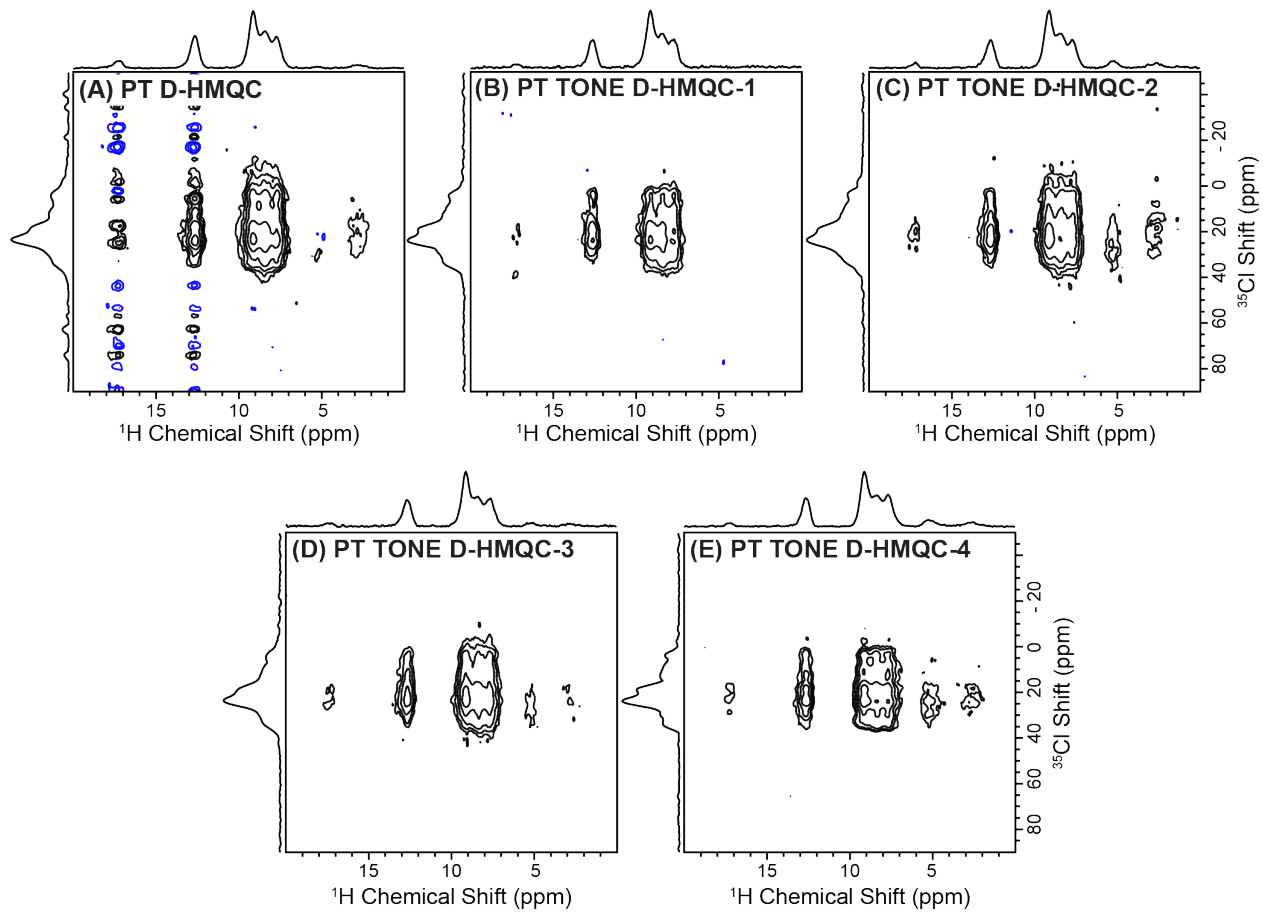


Figure S8. 2D $^1\text{H}\{\text{Cl}^{35}\}$ spectra acquired at 18.8 T with (A) population transfer (PT) D-HMQC, (B) PT TONE D-HMQC-1, (C) PT TONE D-HMQC-2, (D) PT TONE D-HMQC-3 and (E) PT TONE D-HMQC-4 pulse sequences. The population transfer scheme²⁻³ was employed in all cases (see Figure S9 for pulse sequences). The 2D spectra were processed with the same contour floor level to aid the visual comparison of signal and noise. Spectra were acquired at 50 kHz MAS and with an 18.8 T applied magnetic field. The recycle delay was set to 2 s ($^1\text{H } T_1 \sim 7.8$ s), number of scans to 16, number of F_1 increments to 128 with a 25 kHz F_1 spectral width.

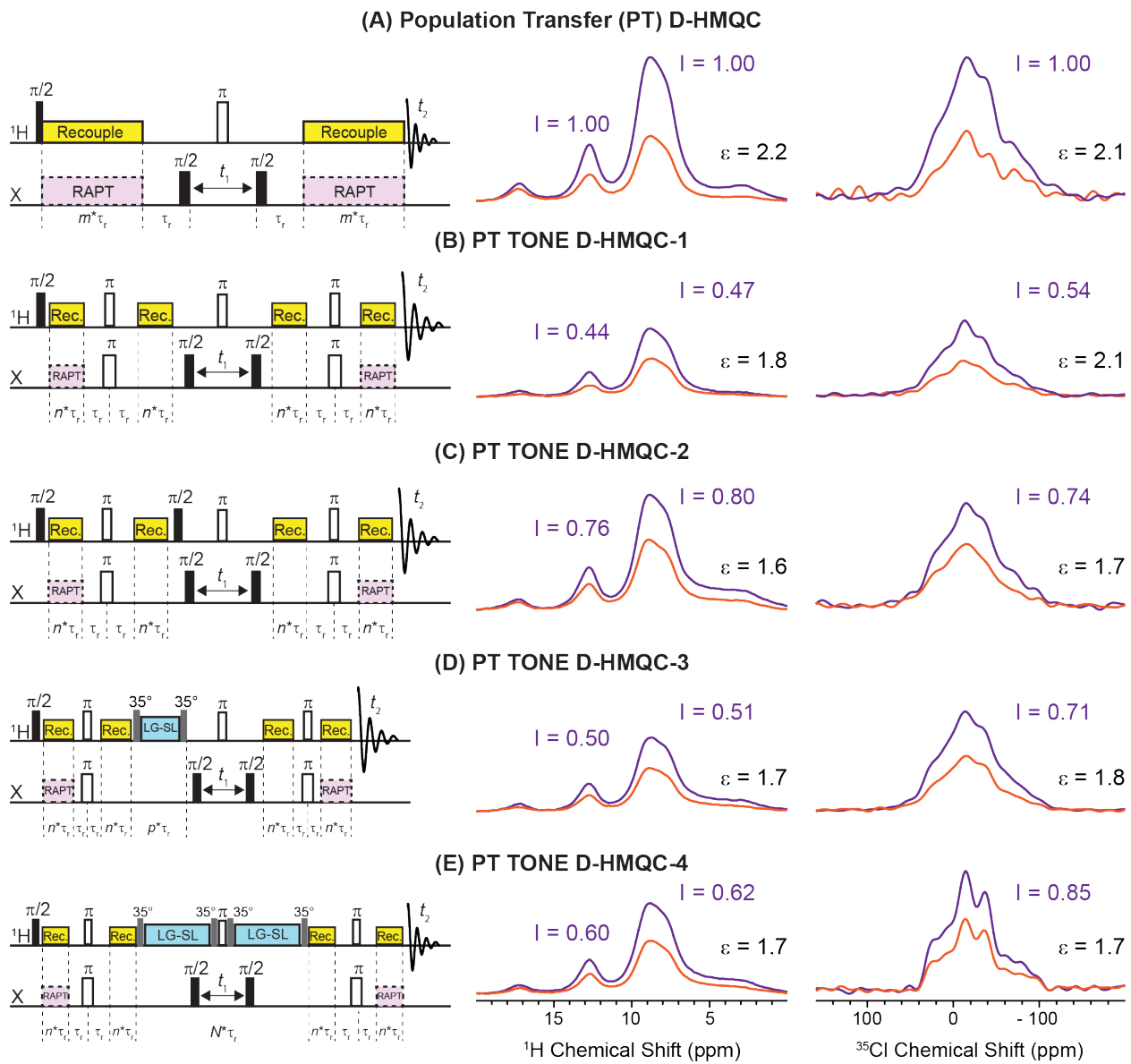


Figure S9. Figure showing incorporation of RAPT pulses to achieve population transfer. (left) Pulse sequences, (center) 1D $^1\text{H}\{\text{Cl}^{35}\}$ D-HMQC spectra and (right) Cl^{35} slices from 2D $^1\text{H}\{\text{Cl}^{35}\}$ D-HMQC spectra at $^1\text{H} \delta = 9.0$ ppm obtained using (A) population transfer (PT) D-HMQC, (B) PT TONE D-HMQC-1, (C) PT TONE D-HMQC-2, (D) PT TONE D-HMQC-3 and (E) PT TONE D-HMQC-4 pulse sequences. Spectra were acquired at 50 kHz MAS and 9.4 T applied magnetic field.

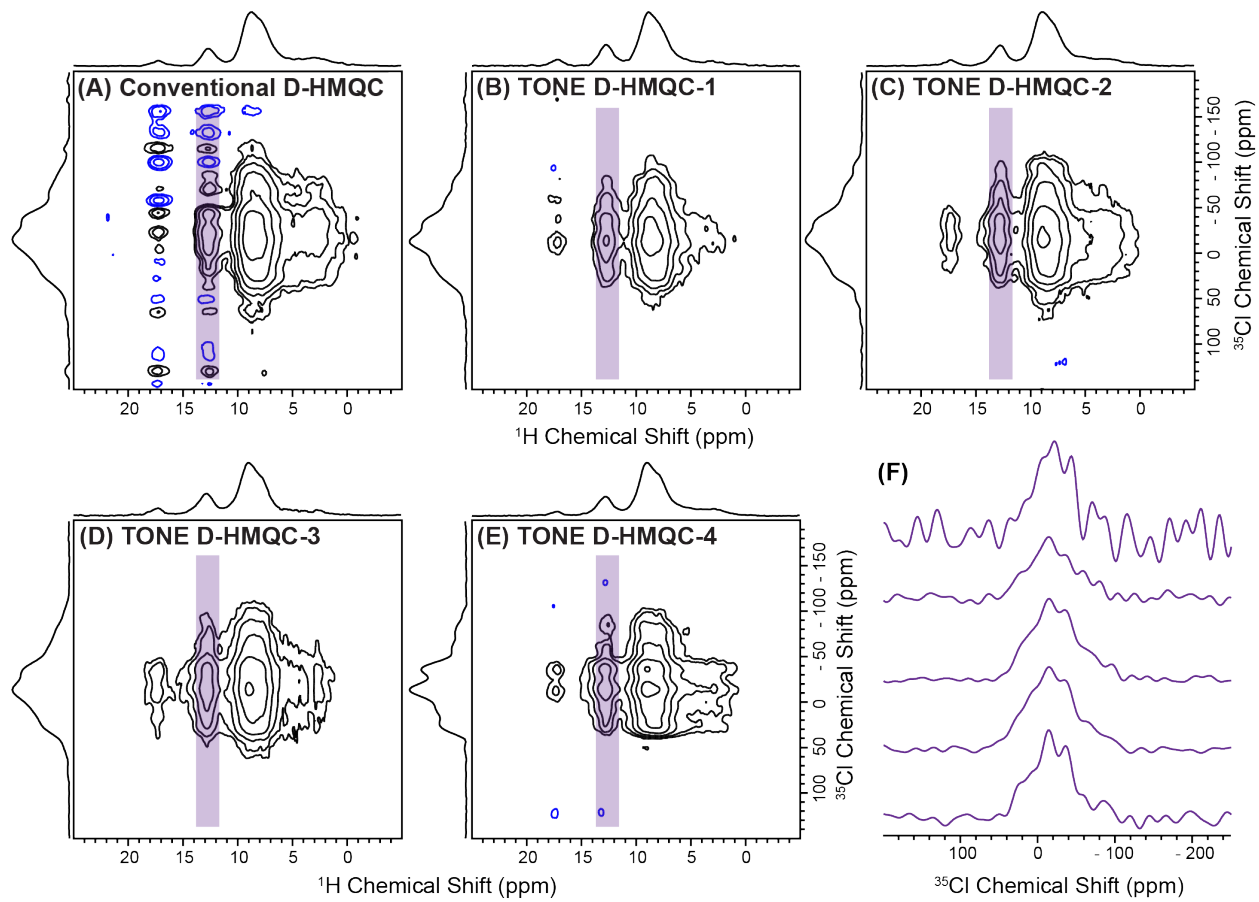


Figure S10. 2D $^1\text{H}\{\text{Cl}^{35}\}$ spectra acquired with (A) population transfer (PT) D-HMQC, (B) PT TONE D-HMQC-1, (C) PT TONE D-HMQC-2, (D) PT TONE D-HMQC-3 and (E) PT TONE D-HMQC-4 pulse sequences. See Figure S9 for pulse sequences. The 2D spectra were processed with the same contour floor level to aid the visual comparison of signal and noise. Spectra were acquired at 50 kHz MAS and 9.4 T applied magnetic field. (F) Cl^{35} traces extracted from 2D $^1\text{H}\{\text{Cl}^{35}\}$ D-HMQC spectra at ^1H δ = 12.7 ppm.

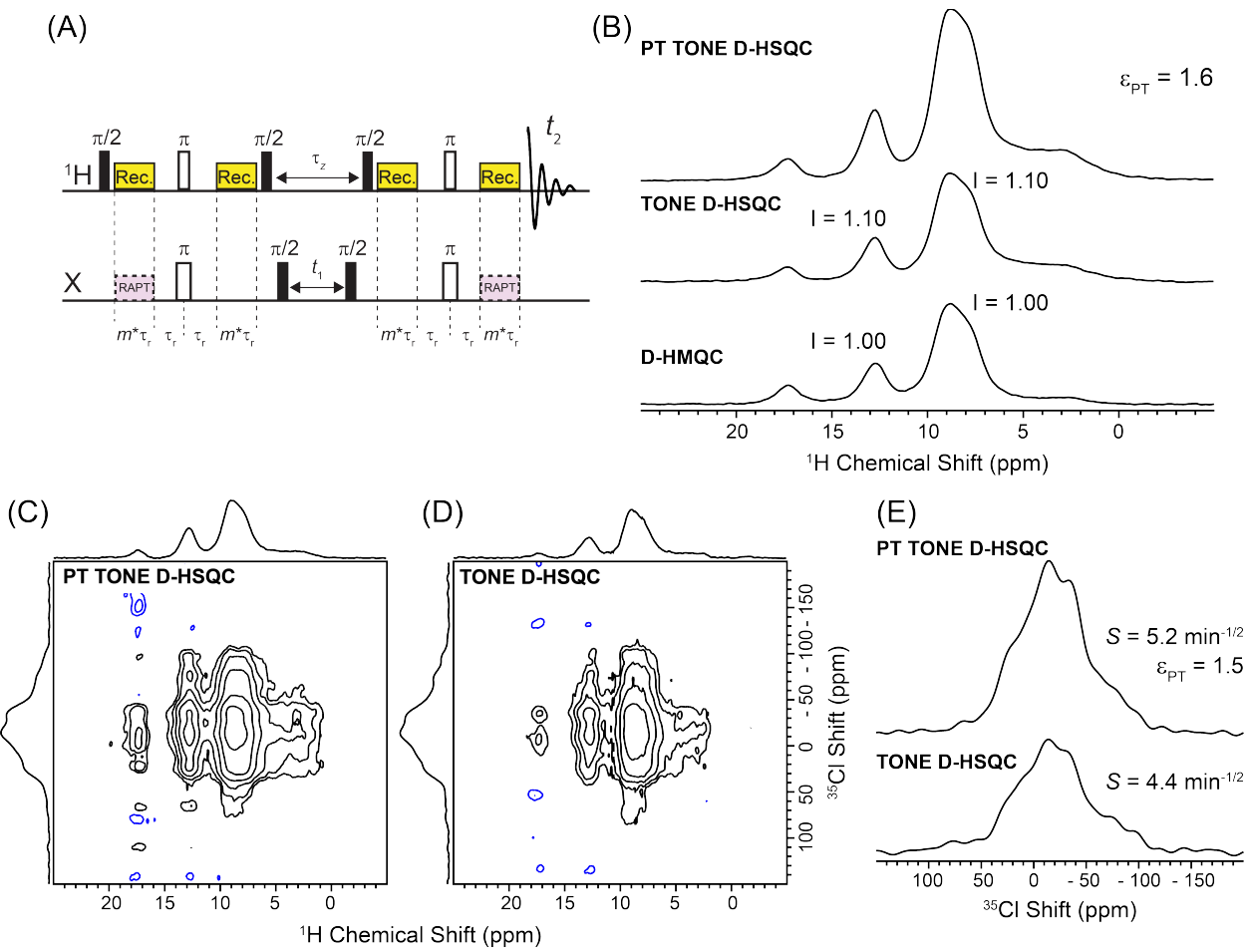
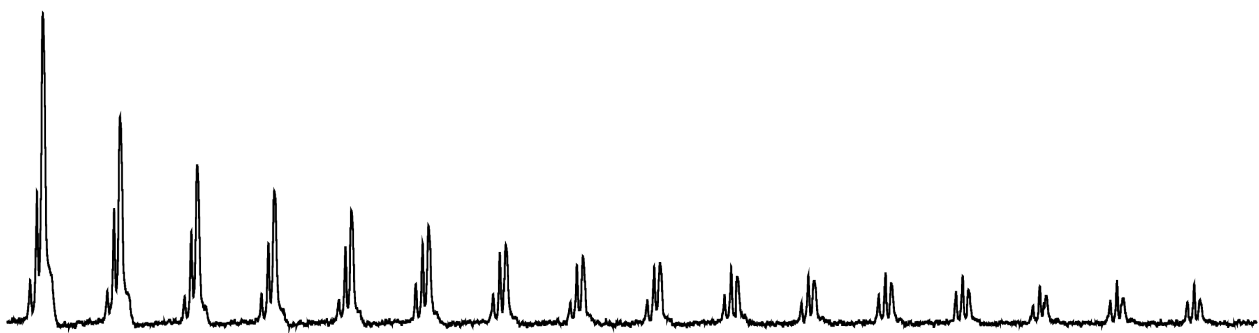


Figure S11. (A) Population transfer (PT) TONE D-HSQC pulse sequence. (B) Comparison of 1D $^1\text{H}\{^{35}\text{Cl}\}$ conventional D-HMQC, TONE D-HSQC and PT TONE D-HSQC spectra. PT provides a gain (ε) of 1.6 for TONE D-HSQC. The relative signal intensities with respect to the conventional D-HMQC is provided. 2D $^1\text{H}\{^{35}\text{Cl}\}$ TONE D-HSQC spectra obtained (C) with and (D) without population transfer. (E) Comparison of ^{35}Cl traces extracted from the 2D spectra shown in (C) and (D) at a $^1\text{H} \delta = 9.0$ ppm. The 2D spectra were processed with the same contour floor level to aid the visual comparison of signal and noise. Spectra were acquired at 50 kHz MAS and 9.4 T applied magnetic field.

(A) TONE D-HSQC



(B) Conventional D-HMQC

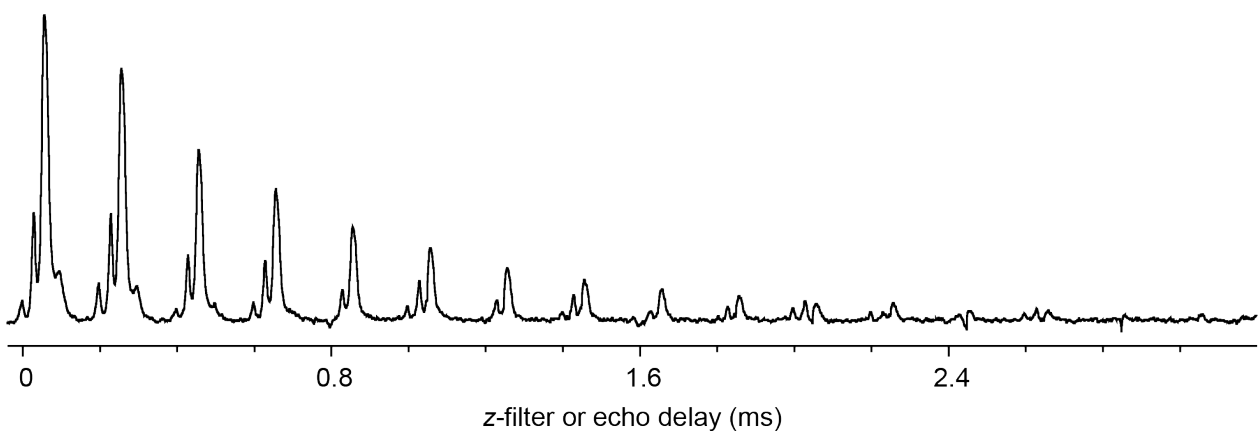


Figure S12. 1D $^1\text{H}\{\text{Cl}^{35}\}$ (A) TONE D-HSQC and (B) conventional D-HMQC spectra acquired by varying the (A) τ_z period shown in Figure S11A and (B) the central echo delay shown in Figure 1A, respectively. Both sets of spectra were obtained with $t_1 = 0$. The MAS frequency was 50 kHz and $B_0 = 9.4$ T.

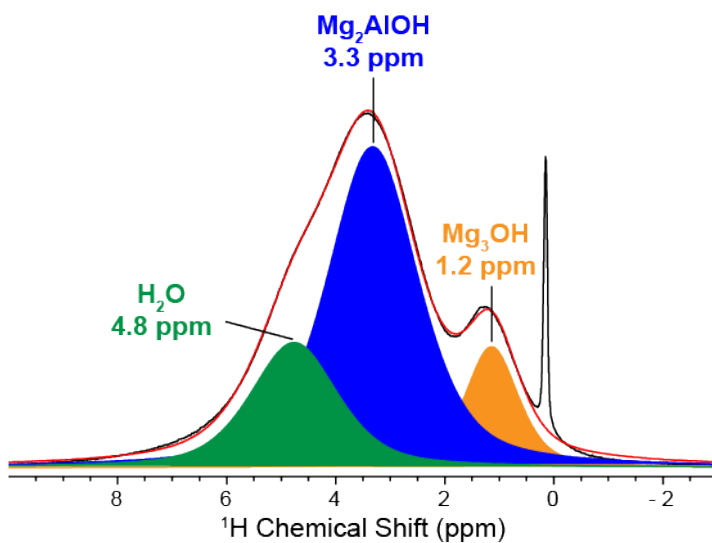
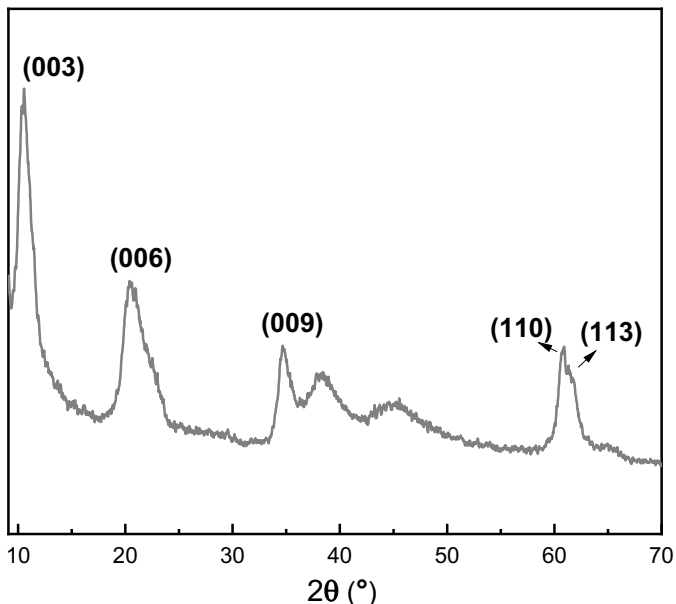


Figure S13. (top) Powder X-ray diffraction pattern of the MgAl-27.8-NO₃⁻ sample. The PXRD pattern confirms the formation of the rhombohedral structure. The peaks observed at 2θ angles of ca. 11°, 21° and 61 correspond to planes (003), (006) and (110). The low intensity peak located at 62.5° corresponds to the plane (113). (bottom) ¹H spin echo NMR spectrum of the LDH sample obtained with 60 kHz MAS and $B_0 = 9.4$ T. The individual ¹H signals are deconvoluted and the ¹H chemical shifts of the different sites are provided in the figure. The sharp signal at 0.15 ppm corresponds to some organic impurities. The relative concentrations of the Mg₂AlOH and Mg₃OH sites are estimated to be 82% and 18%, respectively, based on the integrated signal intensities. The estimated concentrations agree well with a previous report by Yu et al.⁴ Fitting was performed in the Topspin 3.6.1 solid lineshape analysis (sola) module.

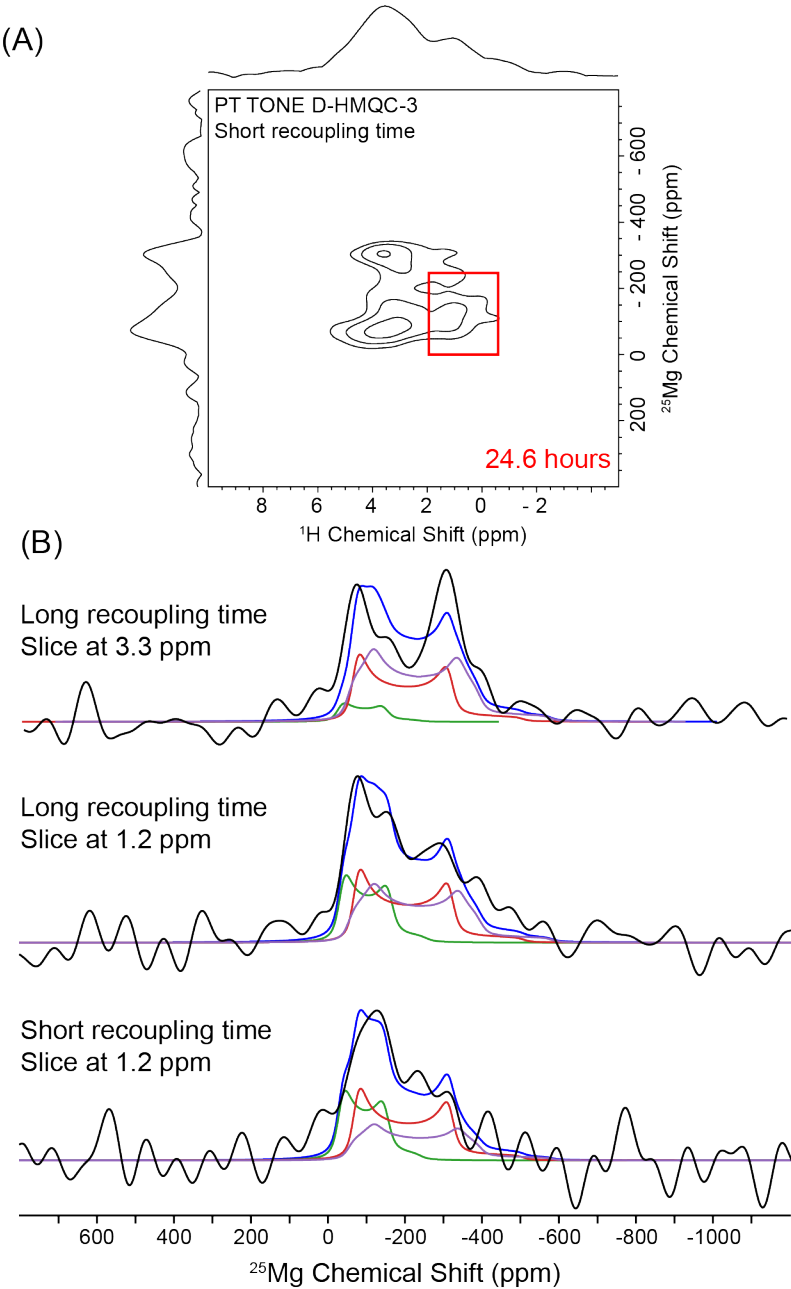


Figure S14. (A) 2D $^1\text{H}\{^{25}\text{Mg}\}$ PT TONE D-HMQC-3 spectrum of MgAl-27.8- NO_3^- obtained with a short (0.8 ms) recoupling duration to selectively observe $^1\text{H}-^{25}\text{Mg}$ proximities (highlighted in red) between protons and magnesium atoms in Mg_3OH (brucite-like) sites. (B) ^{25}Mg slices extracted from (top and middle) the 2D PT TONE D-HMQC-3 spectrum shown in the main text in Figure 4A and (bottom) the 2D PT TONE D-HMQC-3 spectrum shown in (A) at the indicated ^1H chemical shifts. All traces were fit to three different ^{25}Mg sites corresponding to brucite-like $\text{Mg}(\text{OMg})_6$ ($\delta_{\text{iso}} = 2$ ppm, $C_Q = 3.1$ MHz, $\eta = 0.0$), $\text{Mg}(\text{OMg})_3(\text{OAl})_3$ ($\delta_{\text{iso}} = 0$ ppm, $C_Q = 4.5$ MHz, $\eta = 0.0$) and $\text{Mg}(\text{OMg})_4(\text{OAl})_2$ ($\delta_{\text{iso}} = 0$ ppm, $C_Q = 4.8$ MHz, $\eta = 0.2$) based on the previous report by Sideris *et al.* by simply varying the relative integrals.⁵

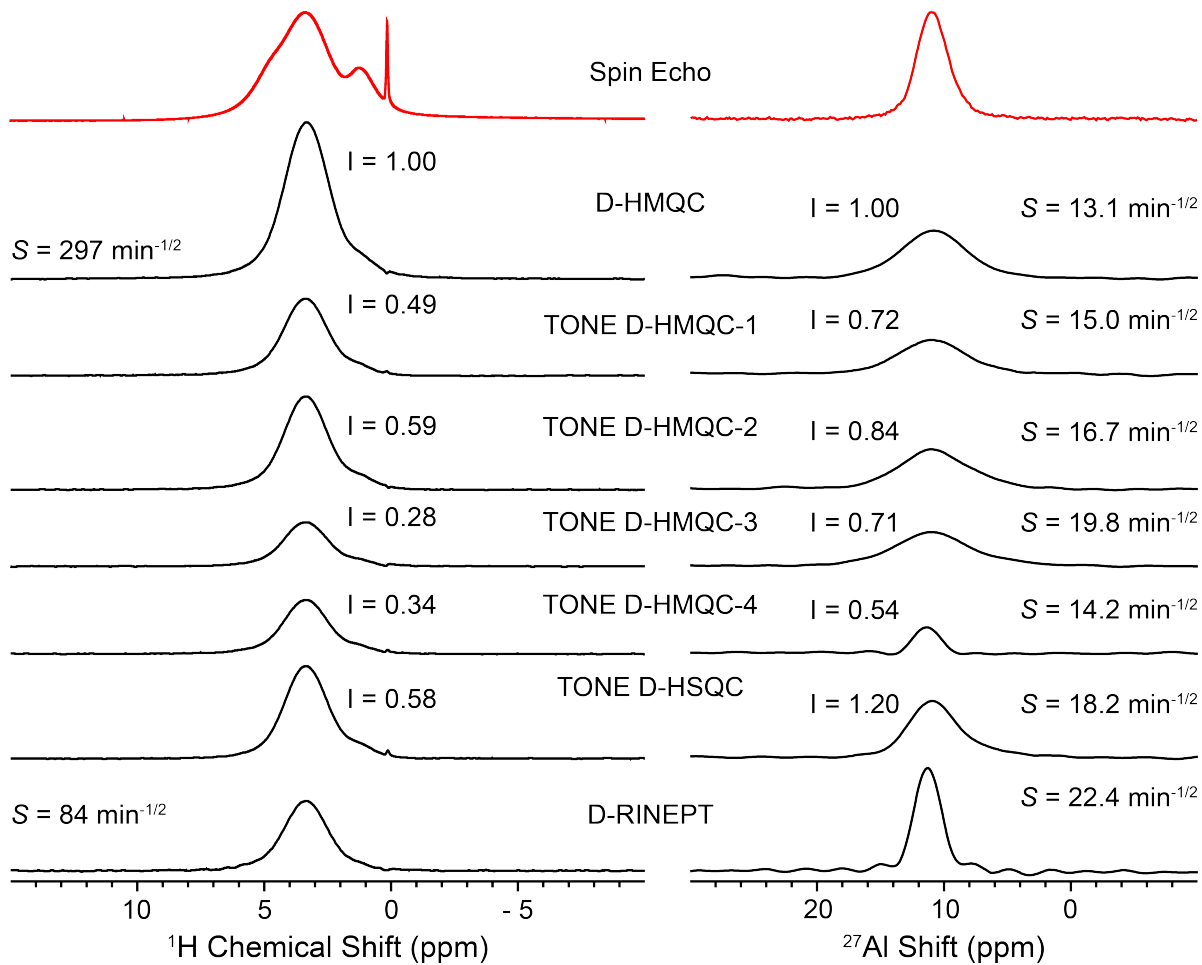


Figure S15. Comparison of (left) 1D proton detected $^1\text{H}\{^{27}\text{Al}\}$ spectra of MgAl-27.8- NO_3^- and (right) ^{27}Al traces extracted from 2D $^1\text{H}\{^{27}\text{Al}\}$ spectra obtained with (top to bottom) conventional D-HMQC, TONE D-HMQC, TONE D-HSQC and $^{27}\text{Al}\rightarrow^1\text{H}$ D-RINEPT pulse sequences. The 1D ^1H and ^{27}Al spin echo spectra are overlaid on top (red traces). Spectra were acquired at 60 kHz MAS and 9.4 T.

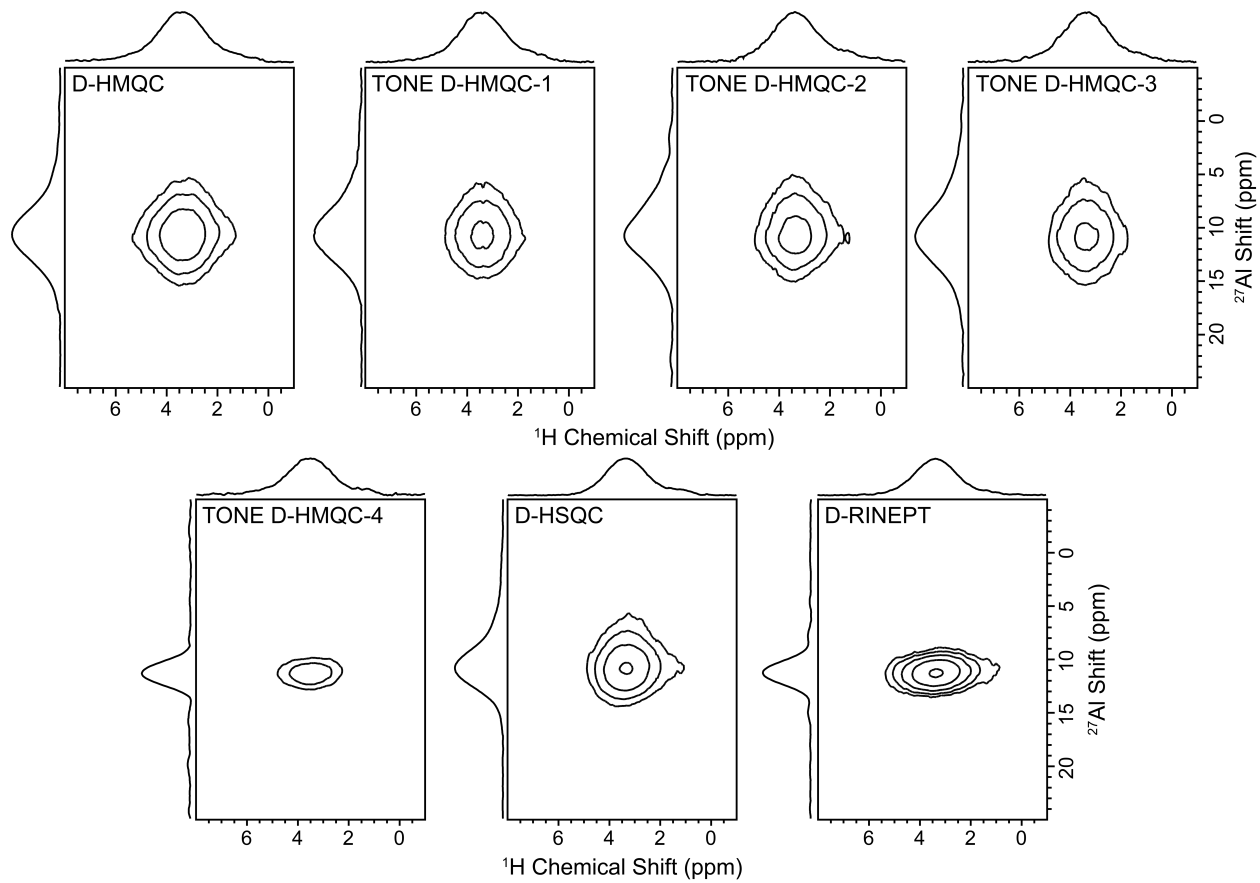


Figure S16. (A) 2D $^1\text{H}\{^{27}\text{Al}\}$ HETCOR spectra of MgAl-27.8- NO_3^- acquired with the pulse sequences indicated in the figure. All spectra were acquired with ^1H detection including the $^{27}\text{Al} \rightarrow ^1\text{H}$ D-RINEPT. Spectra were acquired at 60 kHz MAS and 9.4 T. The 2D spectra were processed with the same contour floor level to aid the visual comparison of signal and noise.

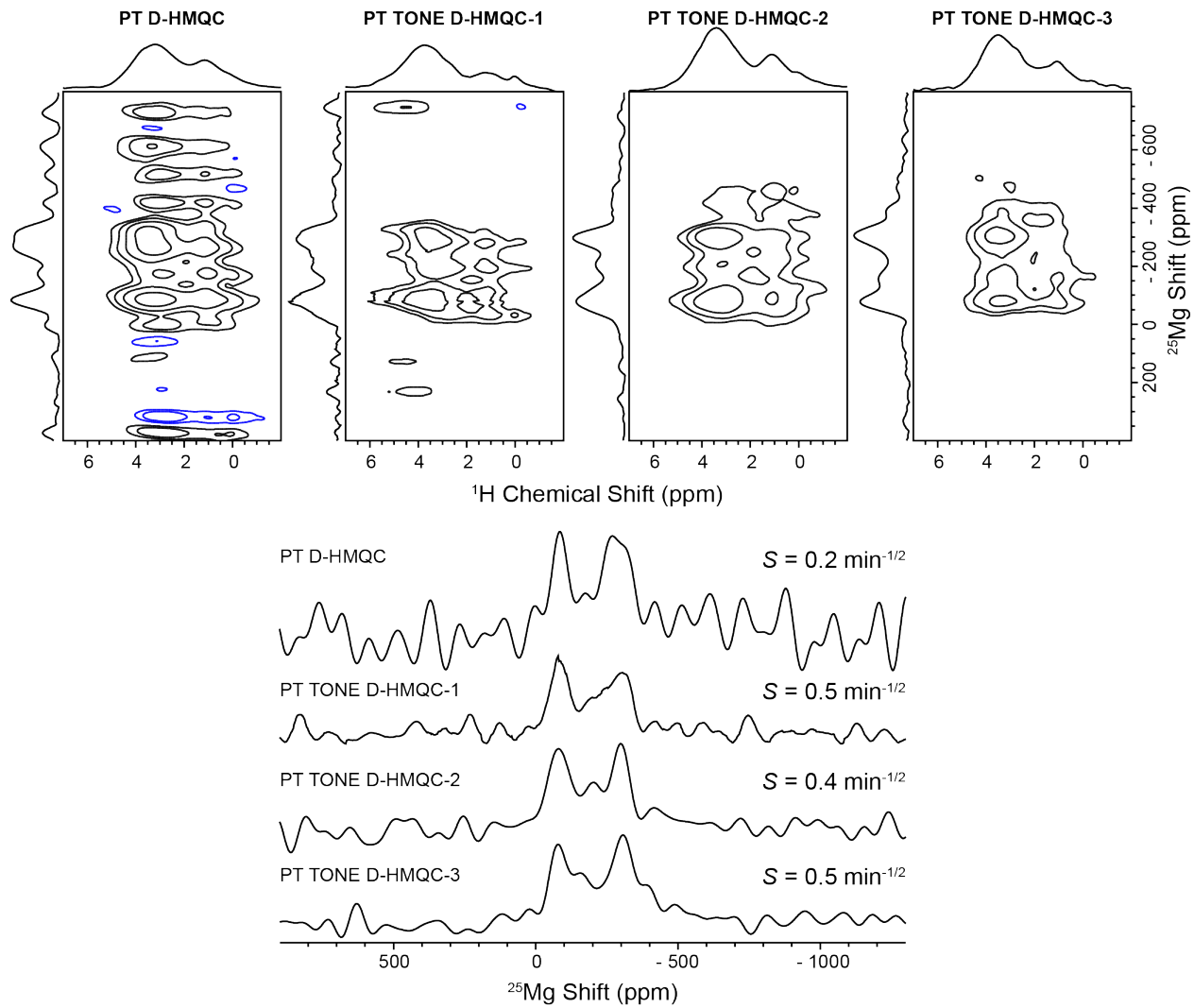


Figure S17. (top, left to right) 2D $^1\text{H}\{\text{²⁵Mg}\}$ PT D-HMQC, PT TONE D-HMQC-1, PT TONE D-HMQC-2 and PT TONE D-HMQC-3 spectra of MgAl-27.8-NO_3^- . (bottom) 1D ^{25}Mg traces extracted from the 2D spectra at a ^1H chemical shift of 3.3 ppm. The 2D spectra were processed with the same contour floor level to aid the visual comparison of signal and noise.

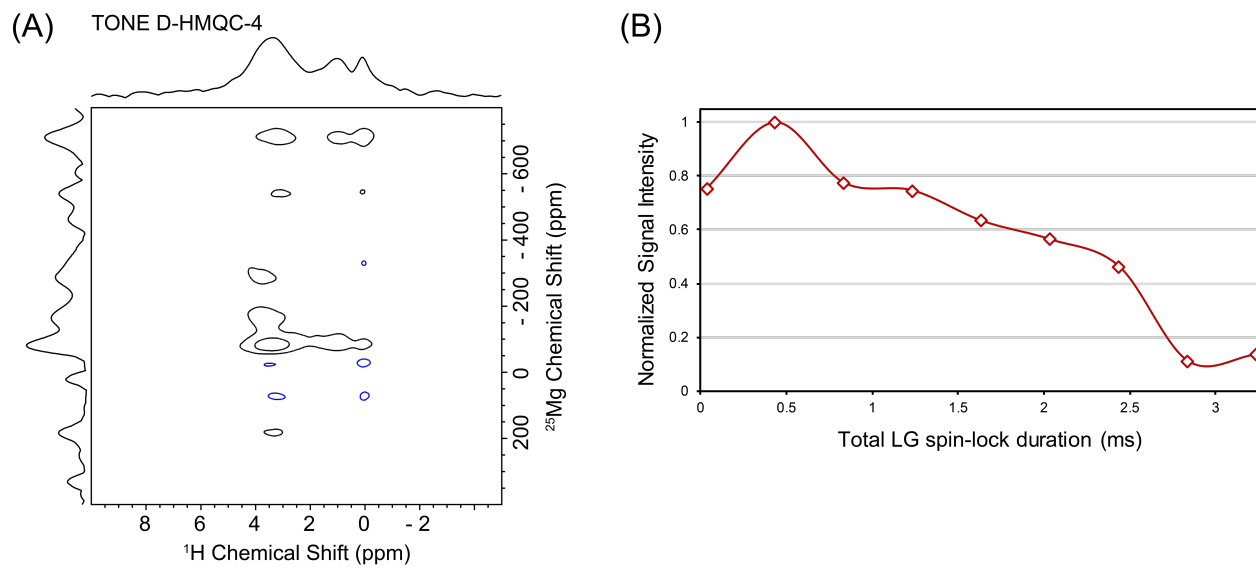


Figure S18. (A) 2D $^1\text{H}\{^{25}\text{Mg}\}$ PT TONE D-HMQC-4 2D of MgAl-27.8- NO_3^- . The total LG spin-lock pulse duration was 60 rotor cycles. (B) Plot showing the decay of the ^1H signal with the total LG spin-lock pulse duration in the $^1\text{H}\{^{25}\text{Mg}\}$ TONE D-HMQC-4 experiment. The MAS frequency was 60 kHz and $B_0 = 9.4$ T.

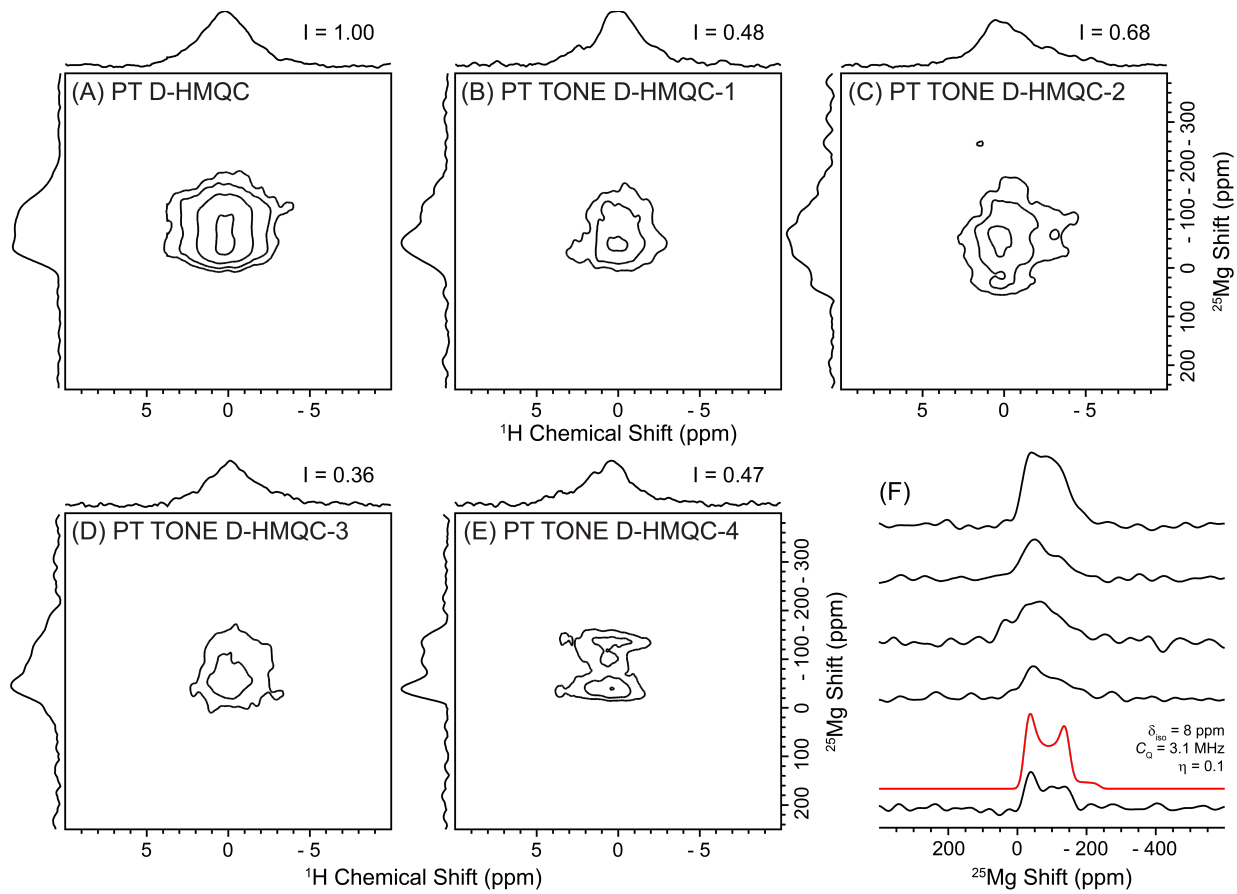


Figure S19. (A-E) 2D $^1\text{H}\{^{25}\text{Mg}\}$ HETCOR spectra of Magnesium Hydroxide acquired with the pulse sequences indicated in the figure. The relative intensities observed with the different D-HMQC sequences in a 1D experiment are indicated above the ^1H projections of the 2D spectra. (F) (top to bottom) Slices extracted from the 2D spectra shown in (A-E). Analytical simulation of the ^{25}Mg second-order quadrupolar pattern is shown in red ($C_Q = 2.1 \text{ MHz}$, $\eta = 0.1$). The 2D spectra were processed with the same contour floor level to aid the visual comparison of signal and noise. Spectra were acquired at 60 kHz MAS and 9.4 T.

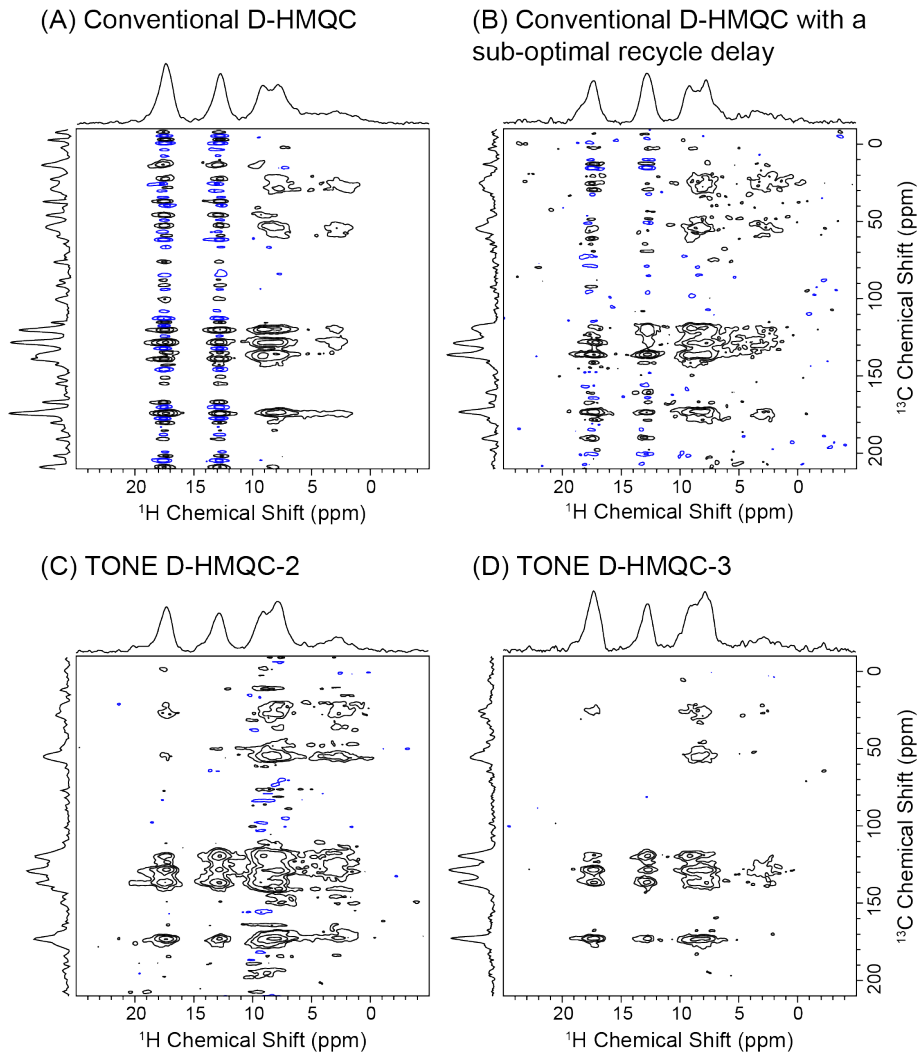


Figure S20. 2D $^1\text{H}\{\text{C}^{13}\}$ (A) conventional D-HMQC, (B) conventional D-HMQC with a sub-optimal (1.05 s) inter-scan delay, (C) TONE D-HMQC-2 and (D) TONE D-HMQC-3 spectra. All spectra were obtained with an MAS frequency of 50 kHz and at $B_0 = 9.4$ T. Spectra shown in (A), (C) and (D) were acquired with 4.2 s inter-scan delay and 16 scans, whereas the spectrum shown in (B) was acquired with 64 scans. 128 t_1 increments were obtained with a F_1 spectral width of 25 kHz in all cases. The total experiment time was the same in all cases (2.39 hours). The 2D spectra were processed with the same contour floor level to aid the visual comparison of signal and noise.

Tables S1-S22: Data from SIMPSON simulations and Lorentz/Gauss Fits of the MAS profiles shown in Figure 2 (main text). The equations used to fit the MAS profiles are provided in the main text. The fitted widths of the Lorentzian (Γ_l) and Gaussian (Γ_g) functions are mentioned in all Table captions. The difference in MAS is calculated in Hz with respect to a 50 kHz MAS frequency. The correlated and uncorrelated signal intensities (real components) are normalized with respect to the intensity of the correlated signal at 50 kHz MAS frequency.

Table S1: Correlated Signal of D-HMQC with ^1H $\delta_{\text{aniso}}=1$ ppm. $\Gamma_g=90$ and $\Gamma_l=1000$.

Difference in MAS	Intensity (real)	Intensity (imaginary)	Normalized Intensity	Total Voigt Fit
-200	-0.123	0.000	-0.236	0.073
-180	-0.045	0.000	-0.086	0.120
-160	0.034	0.000	0.066	0.187
-140	0.113	0.000	0.217	0.277
-120	0.191	0.000	0.368	0.389
-100	0.268	0.000	0.516	0.519
-80	0.343	0.000	0.660	0.657
-60	0.412	0.000	0.793	0.789
-40	0.468	0.000	0.902	0.900
-20	0.506	0.000	0.974	0.974
0	0.519	0.000	1.000	1.000
20	0.506	0.000	0.975	0.974
40	0.469	0.000	0.903	0.900
60	0.413	0.000	0.795	0.789
80	0.344	0.000	0.663	0.657
100	0.270	0.000	0.519	0.519
120	0.192	0.000	0.370	0.389
140	0.114	0.000	0.220	0.277
160	0.036	0.000	0.069	0.187
180	-0.043	0.000	-0.083	0.120
200	-0.121	0.000	-0.233	0.073

Table S2: Correlated Signal of D-HMQC with ^1H $\delta_{\text{aniso}}=10$ ppm. $\Gamma_g=90$ and $\Gamma_l=130$.

Difference in MAS	Intensity (real)	Intensity (imaginary)	Normalized Intensity	Total Voigt Fit
-200	-0.008	0.000	-0.015	0.008
-180	0.017	0.000	0.033	0.016
-160	0.052	0.000	0.101	0.029
-140	0.093	0.000	0.179	0.053
-120	0.128	0.000	0.246	0.093
-100	0.150	0.000	0.290	0.160
-80	0.173	0.000	0.333	0.268
-60	0.229	0.000	0.441	0.432
-40	0.338	0.000	0.651	0.657
-20	0.462	0.000	0.891	0.891
0	0.519	0.000	1.000	1.000

20	0.463	0.000	0.891	0.891
40	0.338	0.000	0.651	0.657
60	0.228	0.000	0.439	0.432
80	0.172	0.000	0.331	0.268
100	0.149	0.000	0.287	0.160
120	0.126	0.000	0.243	0.093
140	0.090	0.000	0.174	0.053
160	0.050	0.000	0.096	0.029
180	0.014	0.000	0.027	0.016
200	-0.011	0.000	-0.022	0.008

Table S3: Correlated Signal of D-HMQC with ^1H $\delta_{\text{aniso}}=17$ ppm. $\Gamma_g=30$ and $\Gamma_t=130$.

Difference in MAS	Intensity (real)	Intensity (imaginary)	Normalized Intensity	Total Voigt Fit
-200	0.078	0.000	0.150	0.000
-180	0.058	0.000	0.112	0.000
-160	0.041	0.000	0.079	0.000
-140	-0.011	0.000	-0.022	0.000
-120	-0.056	0.000	-0.108	0.000
-100	-0.061	0.000	-0.117	0.001
-80	-0.026	0.000	-0.050	0.011
-60	0.029	0.000	0.055	0.073
-40	0.157	0.000	0.303	0.298
-20	0.386	0.000	0.745	0.731
0	0.518	0.000	1.000	1.000
20	0.386	0.000	0.745	0.731
40	0.156	0.000	0.301	0.298
60	0.027	0.000	0.052	0.073
80	-0.027	0.000	-0.051	0.011
100	-0.061	0.000	-0.117	0.001
120	-0.055	0.000	-0.106	0.000
140	-0.008	0.000	-0.016	0.000
160	0.038	0.000	0.073	0.000
180	0.070	0.000	0.136	0.000
200	0.059	0.000	0.114	0.000

Table S4: Correlated Signal of D-HMQC with ^1H $\delta_{\text{aniso}}=34$ ppm. $\Gamma_g=23$ and $\Gamma_t=30$.

Difference in MAS	Intensity (real)	Intensity (imaginary)	Normalized Intensity	Total Voigt Fit
-200	0.021	0.002	0.041	0.000
-180	-0.114	-0.001	-0.221	0.000
-160	0.110	0.001	0.213	0.000
-140	-0.133	0.000	-0.258	0.000
-120	0.128	0.000	0.248	0.000
-100	-0.065	0.000	-0.127	0.000

-80	0.024	0.000	0.046	0.000
-60	0.021	0.000	0.040	0.002
-40	-0.055	0.000	-0.108	0.027
-20	0.135	0.000	0.263	0.247
0	0.515	0.000	1.000	1.000
20	0.135	0.000	0.261	0.247
40	-0.055	0.000	-0.108	0.027
60	0.021	0.000	0.042	0.002
80	0.021	0.000	0.042	0.000
100	-0.026	0.000	-0.051	0.000
120	-0.032	0.000	-0.062	0.000
140	0.127	0.000	0.247	0.000
160	-0.120	0.001	-0.233	0.000
180	0.028	-0.001	0.055	0.000
200	-0.072	0.001	-0.140	0.000

Table S5: Uncorrelated Signal of D-HMQC with ^1H $\delta_{\text{aniso}}=1$ ppm. $\Gamma_g=285$ and $\Gamma_i=275$.

Difference in MAS	Intensity (real)	Intensity (imaginary)	Normalized Intensity	Total Voigt Fit
-200	0.314	0.000	0.605	0.176
-180	0.272	0.000	0.524	0.227
-160	0.246	0.000	0.473	0.288
-140	0.239	0.000	0.460	0.361
-120	0.253	0.000	0.487	0.445
-100	0.286	0.000	0.550	0.540
-80	0.333	0.000	0.641	0.644
-60	0.386	0.000	0.743	0.747
-40	0.434	0.000	0.836	0.838
-20	0.468	0.000	0.901	0.902
0	0.481	0.000	0.925	0.925
20	0.469	0.000	0.902	0.902
40	0.435	0.000	0.837	0.838
60	0.386	0.000	0.744	0.747
80	0.333	0.000	0.642	0.644
100	0.286	0.000	0.551	0.540
120	0.252	0.000	0.486	0.445
140	0.238	0.000	0.458	0.361
160	0.244	0.000	0.470	0.288
180	0.270	0.000	0.520	0.227
200	0.312	0.000	0.600	0.176

Table S6: Uncorrelated Signal of D-HMQC with ^1H $\delta_{\text{aniso}}=10$ ppm. $\Gamma_g=86$ and $\Gamma_i=130$.

Difference in MAS	Intensity (real)	Intensity (imaginary)	Normalized Intensity	Total Voigt Fit
-200	0.110	0.000	0.213	-0.067

-180	0.124	0.000	0.239	-0.060
-160	0.141	0.000	0.271	-0.048
-140	0.156	0.000	0.300	-0.026
-120	0.160	0.000	0.309	0.013
-100	0.152	0.000	0.293	0.078
-80	0.149	0.000	0.288	0.185
-60	0.191	0.000	0.367	0.350
-40	0.296	0.000	0.570	0.578
-20	0.423	0.000	0.814	0.816
0	0.481	0.000	0.927	0.927
20	0.423	0.000	0.815	0.816
40	0.296	0.000	0.570	0.578
60	0.190	0.000	0.366	0.350
80	0.149	0.000	0.287	0.185
100	0.151	0.000	0.292	0.078
120	0.160	0.000	0.308	0.013
140	0.155	0.000	0.299	-0.026
160	0.140	0.000	0.270	-0.048
180	0.123	0.000	0.237	-0.060
200	0.109	0.000	0.211	-0.067

Table S7: Uncorrelated Signal of D-HMQC with ^1H $\delta_{\text{aniso}}=17$ ppm. $\Gamma_g=38$ and $\Gamma_i=90$.

Difference in MAS	Intensity (real)	Intensity (imaginary)	Normalized Intensity	Total Voigt Fit
-200	0.057	0.000	0.109	-0.070
-180	0.043	0.000	0.083	-0.070
-160	0.045	0.000	0.087	-0.070
-140	0.039	0.000	0.076	-0.070
-120	0.058	0.000	0.111	-0.069
-100	0.092	0.000	0.178	-0.065
-80	0.103	0.000	0.199	-0.044
-60	0.078	0.000	0.150	0.033
-40	0.135	0.000	0.261	0.251
-20	0.345	0.000	0.667	0.657
0	0.482	0.000	0.930	0.930
20	0.345	0.000	0.667	0.657
40	0.134	0.000	0.260	0.251
60	0.077	0.000	0.149	0.033
80	0.103	0.000	0.198	-0.044
100	0.092	0.000	0.177	-0.065
120	0.057	0.000	0.109	-0.069
140	0.041	0.000	0.079	-0.070
160	0.040	0.000	0.078	-0.070
180	0.053	0.000	0.101	-0.070
200	0.043	0.000	0.083	-0.070

Table S8: Uncorrelated Signal of D-HMQC with ${}^1\text{H}$ $\delta_{\text{aniso}}=34$ ppm. $\Gamma_g=38$ and $\Gamma_i=90$.

Difference in MAS	Intensity (real)	Intensity (imaginary)	Normalized Intensity	Total Voigt Fit
-200	0.066	-0.001	0.129	-0.057
-180	0.023	0.001	0.045	-0.057
-160	0.012	0.000	0.024	-0.057
-140	0.064	0.000	0.124	-0.057
-120	0.028	0.000	0.054	-0.057
-100	0.031	0.000	0.061	-0.057
-80	0.032	0.000	0.063	-0.056
-60	0.065	0.000	0.127	-0.051
-40	0.089	0.000	0.173	-0.012
-20	0.121	0.000	0.235	0.222
0	0.485	0.000	0.943	0.943
20	0.121	0.000	0.234	0.222
40	0.089	0.000	0.173	-0.012
60	0.065	0.000	0.127	-0.051
80	0.026	0.000	0.050	-0.056
100	0.054	0.000	0.105	-0.057
120	0.024	0.000	0.046	-0.057
140	0.016	0.000	0.031	-0.057
160	0.058	-0.001	0.113	-0.057
180	0.043	0.001	0.084	-0.057
200	-0.019	-0.001	-0.038	-0.057

Table S9: Correlated Signal of TONE D-HMQC-2 with 75° flip-back pulse and ${}^1\text{H}$ $\delta_{\text{aniso}}=1$ ppm. $\Gamma_g=105$ and $\Gamma_i=400$.

Difference in MAS	Intensity (real)	Intensity (imaginary)	Normalized Intensity	Total Voigt Fit
-200	-0.192	0.000	-0.371	0.081
-180	-0.107	0.000	-0.206	0.127
-160	-0.017	0.000	-0.033	0.191
-140	0.073	0.000	0.140	0.276
-120	0.161	0.000	0.310	0.383
-100	0.247	0.000	0.476	0.508
-80	0.329	0.000	0.634	0.645
-60	0.403	0.000	0.777	0.779
-40	0.464	0.000	0.894	0.894
-20	0.505	0.000	0.972	0.972
0	0.519	0.000	1.000	1.000
20	0.505	0.000	0.974	0.972
40	0.466	0.000	0.897	0.894
60	0.405	0.000	0.780	0.779
80	0.331	0.000	0.638	0.645
100	0.249	0.000	0.480	0.508
120	0.163	0.000	0.314	0.383

140	0.075	0.000	0.144	0.276
160	-0.015	0.000	-0.029	0.191
180	-0.105	0.000	-0.202	0.127
200	-0.191	0.000	-0.368	0.081

Table S10: Correlated Signal of TONE D-HMQC-2 with 75° flip-back pulse and ${}^1\text{H } \delta_{\text{aniso}}=10 \text{ ppm}$. $\Gamma_g=120$ and $\Gamma_I=240$.

Difference in MAS	Intensity (real)	Intensity (imaginary)	Normalized Intensity	Total Voigt Fit
-200	-0.004	0.000	-0.008	0.066
-180	0.016	0.000	0.031	0.100
-160	0.047	0.000	0.091	0.148
-140	0.094	0.000	0.181	0.214
-120	0.153	0.000	0.295	0.303
-100	0.219	0.000	0.422	0.417
-80	0.289	0.000	0.558	0.554
-60	0.365	0.000	0.704	0.706
-40	0.439	0.000	0.847	0.851
-20	0.497	0.000	0.957	0.960
0	0.519	0.000	1.000	1.000
20	0.497	0.000	0.958	0.960
40	0.440	0.000	0.848	0.851
60	0.366	0.000	0.706	0.706
80	0.290	0.000	0.560	0.554
100	0.220	0.000	0.423	0.417
120	0.154	0.000	0.296	0.303
140	0.095	0.000	0.183	0.214
160	0.048	0.000	0.093	0.148
180	0.018	0.000	0.034	0.100
200	-0.002	0.000	-0.004	0.066

Table S11: Correlated Signal of TONE D-HMQC-2 with 75° flip-back pulse and ${}^1\text{H } \delta_{\text{aniso}}=17 \text{ ppm}$. $\Gamma_g=85$ and $\Gamma_I=200$.

Difference in MAS	Intensity (real)	Intensity (imaginary)	Normalized Intensity	Total Voigt Fit
-200	0.189	0.000	0.366	0.013
-180	0.141	0.000	0.273	0.025
-160	0.078	0.000	0.150	0.048
-140	0.047	-0.001	0.091	0.087
-120	0.071	0.000	0.138	0.151
-100	0.134	0.000	0.259	0.250
-80	0.212	0.000	0.410	0.392
-60	0.299	0.000	0.577	0.573
-40	0.395	0.000	0.762	0.772
-20	0.481	0.000	0.930	0.935

0	0.518	0.000	1.000	1.000
20	0.482	0.000	0.930	0.935
40	0.395	0.000	0.763	0.772
60	0.299	0.000	0.577	0.573
80	0.212	0.000	0.409	0.392
100	0.133	0.000	0.258	0.250
120	0.070	0.000	0.135	0.151
140	0.046	-0.001	0.088	0.087
160	0.077	0.000	0.148	0.048
180	0.141	0.000	0.273	0.025
200	0.190	0.000	0.368	0.013

Table S12: Correlated Signal of TONE D-HMQC-2 with 75° flip-back pulse and ${}^1\text{H}$ $\delta_{\text{aniso}}=34$ ppm. $\Gamma_g=40$ and $\Gamma_l=145$.

Difference in MAS	Intensity (real)	Intensity (imaginary)	Normalized Intensity	Total Voigt Fit
-200	-0.060	0.000	-0.117	0.000
-180	-0.071	0.000	-0.137	0.000
-160	-0.028	0.000	-0.054	0.000
-140	-0.024	0.000	-0.047	0.000
-120	-0.114	-0.002	-0.222	0.003
-100	-0.146	-0.002	-0.284	0.015
-80	-0.047	-0.002	-0.091	0.061
-60	0.095	-0.001	0.186	0.193
-40	0.242	-0.001	0.472	0.465
-20	0.418	0.000	0.814	0.820
0	0.514	0.000	1.000	1.000
20	0.416	0.000	0.811	0.820
40	0.240	0.000	0.468	0.465
60	0.094	-0.001	0.182	0.193
80	-0.048	-0.001	-0.094	0.061
100	-0.147	-0.002	-0.286	0.015
120	-0.114	-0.001	-0.222	0.003
140	-0.024	0.000	-0.046	0.000
160	-0.028	0.000	-0.054	0.000
180	-0.070	0.000	-0.136	0.000
200	-0.059	0.000	-0.114	0.000

Table S13: Uncorrelated Signal of TONE D-HMQC-2 with 75° flip-back pulse and ${}^1\text{H}$ $\delta_{\text{aniso}}=1$ ppm. $\Gamma_g=550$ and $\Gamma_l=550$.

Difference in MAS	Intensity (real)	Intensity (imaginary)	Normalized Intensity	Total Voigt Fit
-200	0.095	0.000	0.183	-0.146
-180	0.080	0.000	0.155	-0.094
-160	0.070	0.000	0.135	-0.042

-140	0.065	0.000	0.126	0.011
-120	0.067	0.000	0.129	0.062
-100	0.074	0.000	0.143	0.111
-80	0.086	0.000	0.165	0.154
-60	0.100	0.000	0.192	0.191
-40	0.113	0.000	0.217	0.219
-20	0.122	0.000	0.235	0.236
0	0.126	0.000	0.242	0.242
20	0.122	0.000	0.236	0.236
40	0.113	0.000	0.217	0.219
60	0.100	0.000	0.192	0.191
80	0.086	0.000	0.165	0.154
100	0.074	0.000	0.142	0.111
120	0.066	0.000	0.128	0.062
140	0.065	0.000	0.125	0.011
160	0.069	0.000	0.133	-0.042
180	0.079	0.000	0.153	-0.094
200	0.094	0.000	0.181	-0.146

Table S14: Uncorrelated Signal of TONE D-HMQC-2 with 75° flip-back pulse and ${}^1\text{H } \delta_{\text{aniso}}=10$ ppm. $\Gamma_g=350$ and $\Gamma_t=300$.

Difference in MAS	Intensity (real)	Intensity (imaginary)	Normalized Intensity	Total Voigt Fit
-200	0.145	0.000	0.279	-0.452
-180	0.100	0.000	0.194	-0.398
-160	0.072	0.000	0.138	-0.336
-140	0.057	0.000	0.109	-0.264
-120	0.049	0.000	0.094	-0.182
-100	0.044	0.000	0.086	-0.093
-80	0.046	0.000	0.090	0.001
-60	0.061	0.000	0.117	0.092
-40	0.087	0.000	0.168	0.170
-20	0.114	0.000	0.220	0.224
0	0.126	0.000	0.243	0.243
20	0.114	0.000	0.220	0.224
40	0.087	0.000	0.168	0.170
60	0.060	0.000	0.116	0.092
80	0.046	0.000	0.089	0.001
100	0.044	0.000	0.085	-0.093
120	0.048	0.000	0.093	-0.182
140	0.056	0.000	0.109	-0.264
160	0.071	0.000	0.137	-0.336
180	0.100	0.000	0.192	-0.398
200	0.144	0.000	0.277	-0.452

Table S15: Uncorrelated Signal of TONE D-HMQC-2 with 75° flip-back pulse and ^1H $\delta_{\text{aniso}}=17$ ppm. $\Gamma_g=200$ and $\Gamma_l=190$.

Difference in MAS	Intensity (real)	Intensity (imaginary)	Normalized Intensity	Total Voigt Fit
-200	0.126	0.000	0.243	-0.645
-180	0.098	0.000	0.189	-0.611
-160	0.064	0.000	0.123	-0.567
-140	0.036	0.000	0.070	-0.510
-120	0.020	0.000	0.039	-0.434
-100	0.007	0.000	0.014	-0.338
-80	-0.004	0.000	-0.008	-0.216
-60	0.004	0.000	0.007	-0.073
-40	0.044	0.000	0.085	0.076
-20	0.100	0.000	0.192	0.196
0	0.126	0.000	0.244	0.244
20	0.099	0.000	0.192	0.196
40	0.043	0.000	0.084	0.076
60	0.003	0.000	0.005	-0.073
80	-0.005	0.000	-0.009	-0.216
100	0.007	0.000	0.013	-0.338
120	0.020	0.000	0.039	-0.434
140	0.036	0.000	0.070	-0.510
160	0.063	0.000	0.122	-0.567
180	0.098	0.000	0.189	-0.611
200	0.125	0.000	0.242	-0.645

Table S16: Uncorrelated Signal of TONE D-HMQC-2 with 75° flip-back pulse and ^1H $\delta_{\text{aniso}}=34$ ppm. $\Gamma_g=300$ and $\Gamma_l=90$.

Difference in MAS	Intensity (real)	Intensity (imaginary)	Normalized Intensity	Total Voigt Fit
-200	0.023	0.000	0.045	-0.713
-180	0.018	-0.001	0.036	-0.702
-160	0.014	0.000	0.027	-0.688
-140	-0.001	0.000	-0.002	-0.667
-120	-0.031	-0.001	-0.061	-0.638
-100	-0.043	-0.002	-0.083	-0.592
-80	-0.051	-0.002	-0.099	-0.519
-60	-0.085	-0.001	-0.166	-0.399
-40	-0.079	-0.001	-0.154	-0.198
-20	0.040	0.000	0.077	0.082
0	0.128	0.000	0.249	0.249
20	0.039	0.000	0.075	0.082
40	-0.080	0.000	-0.156	-0.198
60	-0.086	0.000	-0.168	-0.399
80	-0.051	-0.001	-0.099	-0.519
100	-0.043	-0.002	-0.083	-0.592

120	-0.031	-0.001	-0.060	-0.638
140	0.000	0.000	0.000	-0.667
160	0.014	0.001	0.028	-0.688
180	0.017	0.000	0.034	-0.702
200	0.022	0.000	0.042	-0.713

Table S17: Correlated Signal of TONE D-HMQC-2 with 90° flip-back pulse and ${}^1\text{H} \delta_{\text{aniso}}=17$ ppm.
 $\Gamma_g=70$ and $\Gamma_i=300$.

Difference in MAS	Intensity (real)	Intensity (imaginary)	Normalized Intensity	Total Voigt Fit
-200	0.156	0.000	0.301	0.006
-180	0.094	0.000	0.181	0.015
-160	0.013	-0.001	0.026	0.034
-140	-0.022	-0.001	-0.042	0.072
-120	0.016	-0.001	0.031	0.140
-100	0.105	0.000	0.202	0.250
-80	0.208	0.000	0.402	0.405
-60	0.309	0.000	0.598	0.597
-40	0.406	0.000	0.785	0.793
-20	0.486	0.000	0.938	0.943
0	0.518	0.000	1.000	1.000
20	0.486	0.000	0.938	0.943
40	0.406	0.000	0.785	0.793
60	0.309	0.000	0.598	0.597
80	0.208	0.000	0.401	0.405
100	0.104	0.000	0.200	0.250
120	0.014	-0.001	0.028	0.140
140	-0.024	-0.001	-0.046	0.072
160	0.012	-0.001	0.024	0.034
180	0.094	0.000	0.181	0.015
200	0.157	0.000	0.303	0.006

Table S18: Correlated Signal of TONE D-HMQC-2 with 80° flip-back pulse and ${}^1\text{H} \delta_{\text{aniso}}=17$ ppm.
 $\Gamma_g=77$ and $\Gamma_i=230$.

Difference in MAS	Intensity (real)	Intensity (imaginary)	Normalized Intensity	Total Voigt Fit
-200	0.178	0.000	0.344	0.009
-180	0.126	0.000	0.242	0.019
-160	0.056	0.000	0.109	0.039
-140	0.024	-0.001	0.047	0.077
-120	0.053	-0.001	0.103	0.142
-100	0.125	0.000	0.241	0.245
-80	0.211	0.000	0.407	0.393
-60	0.302	0.000	0.584	0.580
-40	0.399	0.000	0.770	0.779

-20	0.483	0.000	0.932	0.938
0	0.518	0.000	1.000	1.000
20	0.483	0.000	0.933	0.938
40	0.399	0.000	0.770	0.779
60	0.302	0.000	0.583	0.580
80	0.210	0.000	0.406	0.393
100	0.124	0.000	0.239	0.245
120	0.052	-0.001	0.100	0.142
140	0.023	-0.001	0.044	0.077
160	0.056	0.000	0.107	0.039
180	0.126	0.000	0.243	0.019
200	0.179	0.000	0.346	0.009

Table S19: Correlated Signal of TONE D-HMQC-2 with 60° flip-back pulse and ^1H $\delta_{\text{aniso}}=17$ ppm. $\Gamma_g=140$ and $\Gamma_l=150$.

Difference in MAS	Intensity (real)	Intensity (imaginary)	Normalized Intensity	Total Voigt Fit
-200	0.220	0.000	0.425	0.044
-180	0.185	0.000	0.357	0.065
-160	0.136	0.000	0.262	0.094
-140	0.110	0.000	0.212	0.135
-120	0.122	0.000	0.235	0.195
-100	0.161	0.000	0.311	0.279
-80	0.216	0.000	0.417	0.397
-60	0.289	0.000	0.558	0.556
-40	0.384	0.000	0.742	0.747
-20	0.477	0.000	0.922	0.924
0	0.518	0.000	1.000	1.000
20	0.478	0.000	0.923	0.924
40	0.384	0.000	0.743	0.747
60	0.289	0.000	0.557	0.556
80	0.215	0.000	0.416	0.397
100	0.160	0.000	0.310	0.279
120	0.121	0.000	0.233	0.195
140	0.109	0.000	0.210	0.135
160	0.135	0.000	0.261	0.094
180	0.185	0.000	0.357	0.065
200	0.221	0.000	0.427	0.044

Table S20: Uncorrelated signal of TONE D-HMQC-2 with 90° flip-back pulse and ^1H $\delta_{\text{aniso}}=17$ ppm. $\Gamma_g=110$ and $\Gamma_l=300$.

Difference in MAS	Intensity (real)	Intensity (imaginary)	Normalized Intensity	Total Voigt Fit
-200	0.080	0.000	0.154	-0.930
-180	0.050	0.000	0.096	-0.891

-160	0.008	-0.001	0.015	-0.836
-140	-0.024	-0.001	-0.047	-0.761
-120	-0.041	-0.001	-0.079	-0.662
-100	-0.054	-0.001	-0.105	-0.541
-80	-0.070	0.000	-0.135	-0.401
-60	-0.074	0.000	-0.144	-0.256
-40	-0.053	0.000	-0.103	-0.125
-20	-0.017	0.000	-0.034	-0.032
0	0.001	0.000	0.001	0.001
20	-0.018	0.000	-0.035	-0.032
40	-0.055	0.000	-0.106	-0.125
60	-0.076	0.000	-0.147	-0.256
80	-0.071	0.000	-0.138	-0.401
100	-0.055	0.000	-0.106	-0.541
120	-0.042	-0.001	-0.080	-0.662
140	-0.025	-0.001	-0.048	-0.761
160	0.008	0.000	0.014	-0.836
180	0.049	0.000	0.095	-0.891
200	0.079	0.000	0.152	-0.930

Table S21: Uncorrelated signal of TONE D-HMQC-2 with 80° flip-back pulse and ${}^1\text{H}$ $\delta_{\text{aniso}}=17$ ppm. $\Gamma_g=1000$ and $\Gamma_l=190$.

Difference in MAS	Intensity (real)	Intensity (imaginary)	Normalized Intensity	Total Voigt Fit
-200	0.111	0.000	0.214	-0.656
-180	0.082	0.000	0.159	-0.622
-160	0.045	0.000	0.087	-0.579
-140	0.016	-0.001	0.032	-0.524
-120	0.000	-0.001	0.000	-0.454
-100	-0.013	0.000	-0.025	-0.364
-80	-0.026	0.000	-0.050	-0.253
-60	-0.022	0.000	-0.043	-0.123
-40	0.012	0.000	0.023	0.013
-20	0.061	0.000	0.118	0.121
0	0.085	0.000	0.164	0.164
20	0.061	0.000	0.117	0.121
40	0.011	0.000	0.021	0.013
60	-0.023	0.000	-0.045	-0.123
80	-0.027	0.000	-0.051	-0.253
100	-0.014	0.000	-0.026	-0.364
120	0.000	0.000	0.000	-0.454
140	0.016	-0.001	0.031	-0.524
160	0.045	0.000	0.087	-0.579
180	0.082	0.000	0.158	-0.622
200	0.110	0.000	0.212	-0.656

Table S22: Uncorrelated signal of TONE D-HMQC-2 with 60° flip-back pulse and ^1H $\delta_{\text{aniso}}=17$ ppm. $\Gamma_g=1000$ and $\Gamma_l=155$.

Difference in MAS	Intensity (real)	Intensity (imaginary)	Normalized Intensity	Total Voigt Fit
-200	0.168	0.000	0.324	-0.408
-180	0.142	0.000	0.275	-0.382
-160	0.114	0.000	0.221	-0.348
-140	0.092	0.000	0.177	-0.303
-120	0.076	0.000	0.148	-0.243
-100	0.063	0.000	0.122	-0.162
-80	0.056	0.000	0.108	-0.053
-60	0.075	0.000	0.145	0.089
-40	0.133	0.000	0.257	0.253
-20	0.206	0.000	0.398	0.402
0	0.240	0.000	0.464	0.464
20	0.206	0.000	0.398	0.402
40	0.133	0.000	0.257	0.253
60	0.075	0.000	0.144	0.089
80	0.056	0.000	0.108	-0.053
100	0.063	0.000	0.122	-0.162
120	0.077	0.000	0.148	-0.243
140	0.092	0.000	0.177	-0.303
160	0.114	0.000	0.220	-0.348
180	0.142	0.000	0.274	-0.382
200	0.167	0.000	0.323	-0.408

References:

1. Venkatesh, A.; Hung, I.; Boteju, K. C.; Sadow, A. D.; Gor'kov, P. L.; Gan, Z. H.; Rossini, A. J. Suppressing H-1 Spin Diffusion in Fast MAS Proton Detected Heteronuclear Correlation Solid-State NMR Experiments. *Solid State Nucl Mag* **2020**, 105.
2. Wang, Q.; Li, Y. X.; Trebosc, J.; Lafon, O.; Xu, J.; Hu, B. W.; Feng, N. D.; Chen, Q.; Amoureaux, J. P.; Deng, F. Population transfer HMQC for half-integer quadrupolar nuclei. *J. Chem. Phys.* **2015**, 142 (9).
3. Venkatesh, A.; Hanrahan, M. P.; Rossini, A. J. Proton detection of MAS solid-state NMR spectra of half-integer quadrupolar nuclei. *Solid State Nucl. Magn. Reson.* **2017**, 84, 171-181.
4. Yu, G. Y.; Shen, M.; Wang, M.; Shen, L.; Dong, W. H.; Tang, S.; Zhao, L.; Qi, Z.; Xue, N. H.; Guo, X. F.; Ding, W. P.; Hu, B. W.; Peng, L. M. Probing Local Structure of Layered Double Hydroxides with H-1 Solid-State NMR Spectroscopy on Deuterated Samples. *J Phys Chem Lett* **2014**, 5 (2), 363-369.
5. Sideris, P. J.; Blanc, F.; Gan, Z. H.; Grey, C. P. Identification of Cation Clustering in Mg-Al Layered Double Hydroxides Using Multinuclear Solid State Nuclear Magnetic Resonance Spectroscopy. *Chemistry of Materials* **2012**, 24 (13), 2449-2461.